VILNIUS UNIVERSITY

Valdas Jasaitis

COMPUTER MODELING OF SELF-ORDERED FRONTS UNDER OSCILLATING ZERO-MEAN FORCES

Doctoral dissertation
Physical sciences, informatics (09 P)

Vilnius, 2012

The doctoral dissertation was prepared at Vilnius University in 2006 – 2011.

Scientific supervisor:
prof. habil. dr. Feliksas Ivanauskas (Vilnius University, physical sciences, informatics – 09P)

Consultant:
doc. dr. Ričardas Bakanas (Semiconductor Physics Institute, Center for Physical Sciences and Technology, physical sciences, physics – 02P)

Table of contents

1. Introduction

1.1 Field of the research and relevance of the problem

Spatio-temporal control of both the point-particles and self-ordered structures by use of the time-dependent oscillatory fields of zero-time average, either deterministic (temporally regular) or noisy (temporally irregular) ones, has today become a fundamental field of multidisciplinary research in a wide variety of the highly nonlinear systems of the different physical origin, ranging from biology to physics. The concept of a "force–free" motion, under the generic name of "ratchet-like transport", has provided a new possibility of controlling both the point particles (electrons, atoms, molecules, etc.) and the self-ordered front-structures without any net external force. The "self-propelling" devices, the so-called ratchets, perform work by applying the oscillatory force of zero-time average, either noisy or deterministic one [1]. An intriguing property of the systems performing the ratchet-like shuttling of the self-ordered fronts is their capability to rectify the oscillatory motion of the ac driven front even in the case of the spatially uniform system, by contrast to the ordinary ratchets performing the unforced dc motion of the free particles in the systems lacking the spatial inversion symmetry. The unforced dc drift of the self-ordered fronts (so-called *ratchet effect*) usually originates due to the "hidden" asymmetry of the system, or it comes from the broken temporal symmetry of the oscillatory force acting on the front in the system [2].

Analytical solutions for the governing equations, describing ratchet-like transport of the self-ordered front-structures, are known for very limited cases (i.e., perturbation theory, adiabatic approximation). Moreover, only sine-Gordon [3], cubic polynomial [4] and pseudolinear [5] models have analytical solution of free (unperturbed) self-ordered front-structures. Therefore, more general solutions are obtained using numerical methods on computers, namely, computer modeling: the mathematical model of the considered system is approximated using numerical methods and implemented as a program. Hence, computer modeling has become a very useful method to simulate and analyze

ratchet-like transport in wide ranges of parameter values. Moreover, the ever rapidly improving computer power allows extremely precise numerical experiments uncovering new aspects of the ratchet effect.

In the present research the ratchet-like transport of the self-ordered fronts that result from the competition between the nonlinearity and diffusion are investigated. More exactly, the "bistable" fronts (BFs), which perform the transition from the least stable to the most stable state of the system of the reaction-diffusion type, are examined within the considered model. A crucial factor for the existence of the unforced dc motion of the self-ordered fronts is dissipation, which leads to the temporal irreversibility of the dynamical equations. The self-ordered fronts in the essentially dissipative systems of the reaction-diffusion type driven by noisy (randomly fluctuating) and deterministic (periodically oscillating) zero-average ac forces has been studied in numerous papers, [2, 6-14] and [15-18], respectively.

The focus of the research is to study new possibilities of controlling the directed transport of the dissipative front without any net external force using numerical simulations and analytic tools. There are two different mechanisms for controlling the "unforced" unidirectional net motion of the ac driven front: parametrically stimulated and directly induced. The parametrically stimulated dc drift comes through the action of the external oscillatory field of zero-time average on the externally controllable parameter of the system: the external time-symmetric field acting on the system is transformed into the asymmetrically oscillating force of a finite time average, that pushes the front in the system [2, 6-11]. In other words, the ratchet-like transport takes place when the external time-symmetric field acting on the system is converted (transformed) into the asymmetrically oscillating force of a finite time average, acting on the front in the system. In case of the directly induced dc motion, the ratchet-like transport is derivable by the additive zero-average force acting on the front in the system [12-18]. Numerical methods are used to analyze BF propagation induced by quasi-periodic and bounded noise additive forces of zero-time average.

Ratchet-like transport phenomena, where a net motion of self-ordered structures is induced by deterministic or stochastic zero-average forces, is important not only for academic interests but for practical applications as well. Several new experiments based on the Josephson effect are being suggested and studied, such as voltage rectification by a superconducting quantum interference device (SQUID) ratchet [19], a kink or discrete soliton corresponding to a moving vortex (fluxon, magnetic flux quantum) in a long Josephson junction [20-22], or controlling vortex motion in Josephson junction arrays [23-25]. The advantages of Josephson junction based ratchets are quite easy experimental realization and ability to capture and rectify noise very fast in a broad frequency range; moreover, it is usually described by a perturbed sin-Gordon equation. Additionally, coupled electronic elements (nonlinear resonators) have been used to demonstrate experimentally the existence of noise-enhanced propagation of the self-ordered fronts propagating into metastable state of the bistable system [26, 27].

1.2 Object of the research

The object of this research is mathematical and numerical models describing self-ordered bistable fronts under deterministic and noisy oscillatory fields of zero-time average. Models in the dissertation are formulated by parabolic partial differential equations (PDE) and solved numerically using explicit finite difference method. Computer software was implemented to solve numerical models.

1.3 Objectives and tasks of the research

The objective of this research is to investigate new possibilities of controlling the directed net motion of the self-ordered bistable fronts by the deterministic and stochastic zero-mean ac forces using computer modelling. The following tasks were completed to achieve the objective:

1. Select and apply mathematical and computer models for BFs under deterministic and noisy oscillatory zero-mean fields. Develop computer software for simulating behavior of the BF under additive zero-average forces.
2. Investigate the influence of the retardation effects (time lags) on the spurious drift of the periodically forced BF. Perform computer modeling and compare obtained results using perturbation theory and adiabatic approximation.
3. Perform computer modeling and analyze the effect of the temporally irregular field oscillations on the ratchet-like shuttling of the ac driven front when field is approximated by bi-harmonic function.
4. Perform computer modeling and investigate the performance of the ratchet-like shuttling of the BF derivable by the quasi-periodic zero-average fields of the different spectral content. Considered fields are approximated by multi-harmonic functions.
5. Perform computer modeling and investigate possibilities of controlling the directed net motion of BFs by use of the zero-average bounded noise fields with a changing noise spectrum.

1.4 Research methods

The model considered in the dissertation was formulated by nonlinear parabolic PDE. Then different oscillating field functions were selected and applied. The equations of the mathematical model were approximated by the method of explicit finite difference. The computer-aided simulations were used to investigate properties of the ratchet-like transport of the BFs.

1.5 Results and scientific innovation of the work

1. The mathematical and computer models for the ratchet-like transport of the BF were applied. The computer software for investigation of the BFs being subjected to the oscillatory fields was developed.
2. The influence of the retardation effects (time lags) on the ratchet-like transport of the ac driven fronts was investigated, performing computer simulations. Results were compared using perturbation theory and adiabatic approximation. Role of the symmetry of the rate function on ratchet-like transport was investigated.
3. The performance of the ratchet-like shuttling of the self-ordered BF driven by quasi-periodic, temporally irregular ac fields was investigated using computer modeling. The reversal behavior of the directed net motion of the quasi-periodically forced BFs derivable by the asymmetrical rate functions was analyzed.
4. Oscillatory fields acting on the BF in the system were approximated by the multi-harmonic and bounded noise forcing functions. The performance of the ratchet-like shuttling derivable by the quasi-periodic zero-average fields of the different spectral content was investigated.

1.6 Findings presented for defense

1. The occurrence of the retardation effects (time lags) in the oscillatory motion of the ac driven front shrink the spurious drift of the BF. The effective controlling of the directed net motion of the self-ordered fronts is achieved using the low-frequency zero-mean ac forces.
2. The characteristic relaxation time derivable analytically, by use of the perturbation theory is adequate enough even in case of the strong forcing.

3. The temporally irregular oscillations of the unbiased oscillatory forcing shrink the spurious drift of BF. The optimal, more effective controlling of the directed net motion of BFs is achieved using the periodic ac forcing.
4. The ratchet-like shuttling of the BFs being influenced by the deterministic (quasi-periodic) and noisy ac forces is very sensitive to the spectral content of the oscillatory forcing and rapidly decreases by gradually extending the frequency spectrum of the incommensurable frequency modes.

1.7 Publications and presentations in conferences

Publications in journals:

- V. Jasaitis, F. Ivanauskas, R. Bakanas. Front Dynamics with Delays in a Spatially Extended Bistable System: Computer Simulation, *Nonlinear Analysis: Modeling and Control*, **13**(4), pp. 433–438, 2008.
- R. Bakanas, V. Jasaitis and F. Ivanauskas, Front dynamics with time delays in a bistable system of the reaction-diffusion type: role of the symmetry of the rate function, *Acta Physica Polonica A*, 119(3), pp. 282–293, 2010.
- R. Bakanas, V. Jasaitis and F. Ivanauskas, Self-ordered Front under Temporally Irregular Forcing: Ratchet-like Transport of the Quasi-periodically Forced Front, *Acta Physica Polonica A*, 119(6), pp. 731–739, 2011.

Conference presentations:

- V. Jasaitis, F. Ivanauskas, Front dynamics with delays in a bistable system of the reaction-diffusion type, 2nd International Conference (CHAOS2009) on Chaotic Modeling, Simulation and Applications, Chania, Greece, 2009.

- V. Jasaitis, F. Ivanauskas, Modeling front dynamics in a bistable system of the reaction-diffusion type, In XLIX-th annual Conference of the Lithuanian Mathematical Society, Kaunas, Lithuania, 2008.

1.8 Organization of dissertation

The dissertation is organized as follows. Chapter 2 is a brief introduction to the spatio-temporal control of point particles as it is closely related to the spatio-temporal control of the self-ordered front-structures. Then, the free (unperturbed) traveling self-ordered front-structures are analyzed and expression of the BF velocity is described. Finally, a pseudolinear model and its analytical solution are presented.

Chapter 3 deals with the ratchet-like transport derivable by the additive zero-average forces acting on the BF. First, oscillating forces used for studying control possibilities of the ratchet-like transport are presented. Then, available analytic tools for finding front solutions in special cases are described. Last section is dedicated to the computer modeling where a mathematical model of the given problem is presented. Accordingly, a numerical method and computer algorithm together with implementation are described.

In Chapter 4 results obtained using both the numerical simulations and analytic tools are presented. The chapter is divided into four parts depending on which forcing function was used.

Finally, the main conclusions are summarized in Chapter 5 and a list of references in Chapter 6.

2. Review of point particles and self-ordered fronts

2.1 Spatio-temporal control of point particles

Mechanism of ordinary ratchets, performing the unforced dc motion of the free particles (electrons, atoms, molecules, etc.), is related to the working principle of ratchet-like transport of self-ordered fronts. Therefore, it is important to understand the basic principle behind ratchet-like devices of the point particles. A new possibility of rectifying fluctuations of the zero-time average (i.e. field gradients, spatially varying temperature) in periodic structures with spatial asymmetry (no reflection symmetry) has stimulated interest in such diverse areas as biology, chemistry or physics [28-31]. The interest of such transport mechanisms originated from studying moving protein motors (myosin or kinesin) [28, 29]: Magnasco showed that Brownian particle in a periodic potential with broken symmetry under external force having time correlations (nonwhite noise) can exhibit a nonzero net drift speed. A use of asymmetrical potential was inspired by a purely mechanical Brownian ratchet and pawl system that was introduced by Smoluchowski [32] and was analyzed by Feynman [33] afterwards. Smoluchowski-Feynman ratchet is a small theoretical device that consists of a so-called *ratchet*, a round gear with *asymmetric* saw-teeth and a pawl that restricts the ratchet to turn only in one direction, connected by an axle with paddles that experience the random Brownian motion (Figure 1). A load is connected to the spool and both the ratchet and pawl are isolated in separate heat baths at different temperatures filled with gas molecules. Similarly to the Maxwell's demon [34] that extracts work from a single heat bath, it can be shown that only out of thermal equilibrium, if T_1 was greater than T_2, the system converts Brownian motion into useful work (e.g., lift a load) by acting as a heat engine – the system rectifies random motion of the particles in the system out of thermal equilibrium (Figure 1) [33, 35, 36]. Consequently, in order to produce useful work using the ratchet mechanism the non-equilibrium random fluctuations (usually colored noise) or periodically oscillating forces are needed. Indeed,

the system is of dissipative type and constantly needs energy (external force) to keep moving.

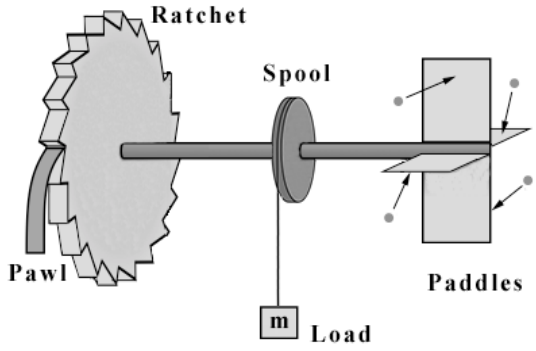

Figure 1. The Smoluchowski-Feynman ratchet. The random collisions of gas molecules (Brownian motion) imparts momentum on the paddles. The ratchet experiences motion in both directions but the pawl allows a systematic rotation in only one direction.

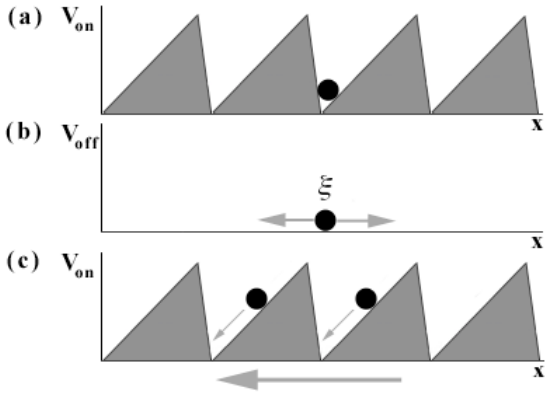

Figure 2. The on/off ratchet mechanism: (a) Brownian particle is trapped in a periodic asymmetric potential V; (b) Particle is spread around the original position due the Brownian motion when the potential is turned off; (c) Particle can be trapped in the asymmetric potential minimum at the right from the original position and or at the left.

From a theoretical point of view, two basic classes of ratchet systems can be distinguished – flashing (pulsating) and rocking (tilting) ratchets. A flashing ratchet has a potential shape depending on time and can be described by the Langevin equation:

$$\{m\,\ddot{x}\} + \eta\,\dot{x} + \sin^2(\omega\,t)\,V'(x) = \xi(t). \qquad (1)$$

In fact, this is the Newton's equation of motion in one dimension that describes a Brownian particle with mass m and coordinate $x(t)$. Typically, the considered system is very small and the inertia term $m\,\ddot{x}$ can be eliminated from the equation (1), the dynamics is overdamped. Here the force $\sin^2(\omega\,t)$ makes the asymmetric ratchet potential $V(x)$ to flash (pulsate). Randomly fluctuating forces equivalent to thermal noise $\xi(t)$ are modeled by a Gaussian white noise of zero average, $\langle\xi(t)\rangle = 0$, and connected to the friction coefficient η satisfying fluctuation-dissipation theorem [37]

$$\langle\xi(t)\xi(s)\rangle = 2\eta k_B T\delta(t-s), \qquad (2)$$

where k_B is the Boltzmann's constant, T is the absolute temperature and δ is Dirac's delta function. In case of the rocking ratchet, a periodic or stochastic

zero-mean additive driving force $f_0 \sin(\omega t)$ makes the ratchet to tilt and can be described as follows:

$$\{m \ddot{x}\} + \gamma \dot{x} + V'(x) + f_0 \sin(\omega t) = \xi(t). \quad (3)$$

The simplest model to explain a working ratchet mechanism is an overdamped Brownian particle in spatially periodic potential with a broken symmetry. This on/off (flashing) ratchet is driven out of thermal equilibrium periodically turning the asymmetric saw-tooth potential on and off: ratchet performs a direct net motion to the left (Figure 2). In fact, the on/off ratchet is a so-called Brownian motor – ordinary ratchet that combines Brownian motion with unbiased external input signals, noisy or deterministic, to achieve direct motion of particles [38-40]. In other words, Brownian motors are small-scale asymmetric objects that are able to rectify fluctuations [28, 41]. Recent experiments related to Brownian motors demonstrated how noise rectification could actually be utilized to effectively control particle transport on the small scale, i.e., nanopores, lithographic tracks, optical traps, superconducting devices, quantum devices and biomolecular motors [42-45]. Due to this, noise and fluctuations can play a constructive role in nonlinear systems and have become a promising technique for studying nanodevices in the non-equilibrium conditions. [46].

2.2 Self-ordered front-structures

The focus of this research is traveling self-ordered front-structures (auto-waves) that are solutions to nonlinear partial differential equations (PDEs) of the parabolic type, namely, the essentially dissipative systems of the reaction-diffusion type. Traveling auto-waves maintain their shape when propagate at constant speed in one direction. Such self-ordered structures arise from the balance between nonlinearity and diffusion far from thermodynamic equilibrium and have been used in many models applied in chemistry, biology, physics, combustion, etc. The scalar reaction-diffusion equation of a single component model in one-dimension settings has a form

$$u_t - u_{xx} + R(u) = 0. \quad (4)$$

Terms u_t and u_{xx} denote a time $t \in \mathbb{R}$ and space $x \in \mathbb{R}$ derivatives, respectively, and a function of concentrations of the diffusing species $u = u(x,t)$ stands for the traveling wave solution. The nonlinear rate (reaction) function $R(u)$ describes the rate of the transient (reaction) processes in the system. Studying the ratchet effect the function $R(u)$ is characterized by the N-shaped R-u dependence with three zeroes at the points $u = u_1,\ u_2,\ u_3$ (Figure 3). In this case the function $R(u)$ can be symmetrically or asymmetrically shaped.

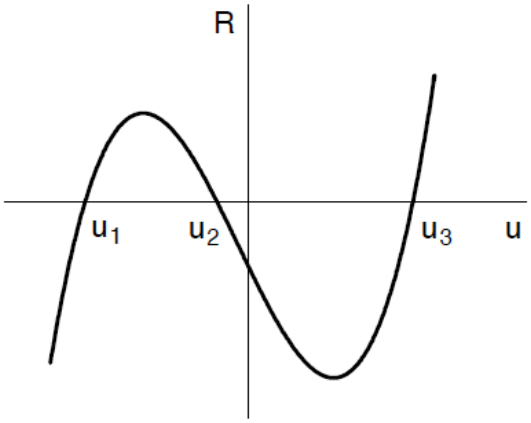

Figure 3. The nonlinear rate function *R(u)* of N-type.
Zeroes of the rate function: u_1, u_2 and u_3.

Traveling front-structures are solutions to (4) of the specific form $u(z,t) = u(x - ct, t)$ with the traveling coordinate $z = x - ct$. They propagate with a constant speed c and have a constant front profile $u(z)$, as it will be proved later. Substituting the (z,t) coordinates into (4) results in the following second-order PDE:

$$u_t - u_{zz} - c\,u_z + R(u) = 0,\ z \in \mathbb{R}. \tag{5}$$

This equation represents the free (undisturbed) traveling auto-wave frame – coordinates travel together with the solution and observe it as a steady one. The field of the ac driven BF $u(z,t)$ must tend to the values $u(z \to -\infty) \to u_1$ and $u(z \to +\infty) \to u_3$.

For the first time a typical nonlinear form of the reaction-diffusion equation was analyzed by Kolmogorov, Petrovsky, and Piskounov (KPP) [47] and, separately, by Fisher [48] back in 1937 to model dispersion of biological populations:

$$R(u) = u(1-u). \tag{6}$$

As one can see, this kinetic function is a quadratic polynomial. Two zeros of the function (6) correspond to stationary states of an active medium where one is stable and second is unstable one. A solution of the equation (4) with the kinetic equation (6) is a single traveling front (so-called Fisher front). This type of equation comes from chemical kinetics (for example, from autocatalytic reactions).

One year later in 1938, Zeldovich and Frank-Kamenetsky proposed a model with a cubic nonlinearity [49]:

$$R(u) = (u-u_1)(u-u_2)(u-u_3),\ u_1 < u_2 < u_3. \tag{7}$$

They investigated flame propagation (combustion theory) in a form of traveling auto-wave front combining reaction-diffusion equation (4) with the kinetic equation (7) that corresponds to autocatalysis of the second order. Additionally, a particular case with $R(u) = u^2(1-u)$ is called Zeldovich equation as well [50]. The cubic polynomial rate function (7) has three zeros which is used to describe bistable active media with two stable stationary states and one bistable state in between acting as a threshold of excitation. It is worth to mention, that depending on the initial conditions fronts can have anti-fronts traveling in opposite direction but the distinction between them is rather artificial. The cubic polynomial model is widely used in theoretical studies of the fronts in physically diverse systems, such as modeling of nerve impulse along bistable transmission lines [51], coupled FitzHugh–Nagumo type of systems to describe nerve pulse transmission [52, 53], Gunn waves that describe electric field transport in semiconductors [54], simple chemical reaction-diffusion systems [55], etc.

To summarize, only sine-Gordon [3], cubic polynomial [4] and pseudolinear [5] models with the rate function $R(u)$ of the N-shape have analytical solution of free (unperturbed) self-ordered front-structures. Pseudolinear model, that is linear approximation of cubic polynomial model (7), is used in this research and is describe in the following sections. Sine-Gordon model describes not only dissipative systems but also energy conserving (non-dissipative) ones and

is expressed as hyperbolic PDE with a Hamiltonian structure:

$$u_{xx} - u_{tt} + \sin(u) = 0 \tag{8}$$

Solution to the Sine-Gordon equation (8) is call topological soliton. However, the unforced dc transport (the ratchet effect) exists only in the presence of dissipation (free energy of the system dissipates) therefore the parabolic PDE (5) is researched further. The dissipation effaces the memory of the system at every time step, i.e., no chemical or physical processes occur after the front-structure has swept through.

2.2.1 Phase portrait

The existence of traveling self-ordered front solutions and analysis of their properties is studied using *phase plane method* – one of the most important techniques for studying the behavior of the nonlinear second-order PDE. If a stationary solution, $u(z) = u(z,t)$, of the equation (5) exists, then it must satisfy the following second-order ordinary differential equation (ODE):

$$u_{zz} + c\, u_z - R(u) = 0 \tag{9}$$

The equation (9) can be transformed to a first-order system of ODEs:

$$\begin{cases} \dfrac{du}{dz} = v \\ \dfrac{du}{dz} = -cv + R(u) \end{cases} \tag{10}$$

To find singular, fixed points, or equilibrium, in the phase plane where system states can stay forever, it is needed to set $\dfrac{du}{dz} = \dfrac{dv}{dz} = 0$. Then the system (10) can be rewritten to

$$\begin{cases} v = 0 \\ -cv + R(u) = 0. \end{cases} \tag{11}$$

Because of the rate function $R(u)$ of the N-type, the above system has three null points:

$$\begin{cases} u_n = u_1,\ u_2,\ u_3 \\ v_n = 0 \end{cases} \tag{12}$$

Linearizing the equation (9) around fixed points $(u_n,\ v_n)$, one arrives to the following mathematical expression:

$$\begin{cases} \dfrac{du}{dz} \approx j_{11}u + j_{12}v = 0\,u + 1\,v \\ \dfrac{dv}{dz} \approx j_{21}u + j_{22}v = R'(u_f)\,u - c\,v \end{cases} \tag{13}$$

As one can see, the matrix J in (13) is the Jacobian matrix evaluated at the fixed points:

$$J = \begin{pmatrix} 0 & 1 \\ R'(u_n) & -c \end{pmatrix} \tag{14}$$

Now we need to find the characteristic polynomial, $\det(J - \lambda I)$, which will be a quadratic equation $\lambda^2 + \sigma\lambda + \delta$. Here I denotes the identity matrix. The classification of the fixed points depends mainly on the characteristic trace parameter

$$\sigma \equiv \frac{j_{11} + j_{22}}{2} = -\frac{c}{2} \tag{15}$$

and the determinant $\delta = \det(J)$ of the matrix J:

$$\delta = \begin{vmatrix} 0 & 1 \\ R'(u_n) & -c \end{vmatrix} = -R'(u_n). \tag{16}$$

The calculated eigenvalues of J, λ_1 and λ_2, can be used to classify fixed points:

$$\lambda_{1,2} = -\frac{c}{2} \pm \sqrt{\frac{c^2}{4} - R'(u_n)} \tag{17}$$

The Figure 4 shows a classification scheme of the fixed points of two-dimensional phase spaces. The values of σ, δ and the parabola $\sigma^2 - 4\delta$ indicates 6 possible types and stability of the fixed points in phase plane (Figure 4): saddle, if $\delta < 0$; stable node, if $\delta > 0$, $\sigma < 0$, $\sigma^2 - 4\delta \geq 0$; unstable node, if $\delta > 0$, $\sigma > 0$, $\sigma^2 - 4\delta \geq 0$; center, if $\delta > 0$, $\sigma = 0$; stable spiral, if $\sigma < 0$, $\sigma^2 - 4\delta < 0$; unstable spiral, if $\sigma > 0$, $\sigma^2 - 4\delta < 0$. Also, the classification can be done using eigenvalues (17).

As a consequence, linearizing around the singular point $(u_1, 0)$ one can see that that the point is a *saddle*. Similarly, linearizing around the singular point $(u_3, 0)$ shows that this point is always a *saddle*. Depending on the velocity c of the traveling front, equilibrium point $(u_2, 0)$ is unstable and can be either *node*

or *focus*:

$$u_2 = \begin{cases} Node, & |c| < |c^*| \\ Focus, & |c| > |c^*| \end{cases} \tag{18}$$

where $|c^*| \equiv -2\sqrt{R'(u_2)}$. In addition, unstable point can be *center* if $c = 0$ but then BF is static, motionless.

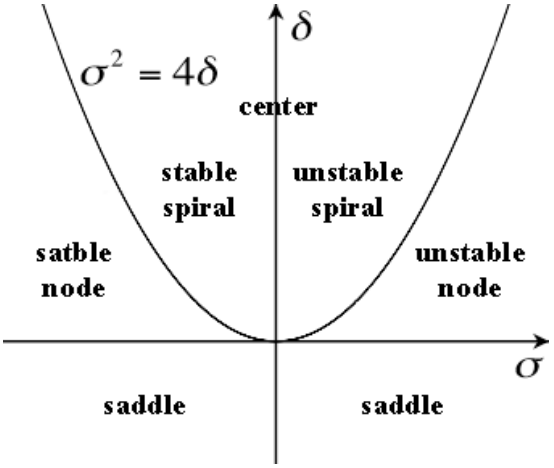

Figure 4. Classification of fixed points for two-dimensional systems.

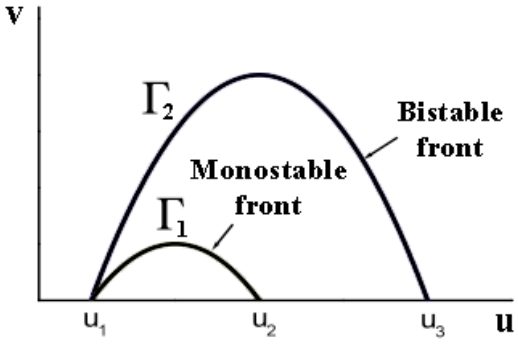

Figure 5. Heteroclinic trajectories in the *u*-*v* phase plane that connects saddle point u_1 with unstable node u_2 and two saddle points u_1 and u_3.

Classification of front structures can be done using phase portrait (Figure 5). Trajectory Γ_1 in the phase plane connects two stationary states, saddle and node. The front is called monostable because transition occurs between stable u_1 and unstable u_2 states (stable state "invades" unstable one). Monostable front (also called Fisher front) corresponds to the Fisher equation (6).

Another type of fornt structure is so-called bistable front (BF) that corresponds to trajectory Γ_2 in the phase plane (Figure 5) connecting two saddle points. Transition occurs between two stable states (stable state u_1 "invades" meta-stable state u_3). It is possible to show by adjusting the front speed c in a $u-v$ phase plane that there is a precisely one value c for which exists a unique connecting trajectory Γ_2 [56]. Front solutions move with constant speed c without changing their shape that is presented in the Figure 6. To achieve BF solution, N-type nonlinear rate function with three zeros can be described by the cubic polynomial function (7), sine function or piecewise-linear function that will be introduced later. This research investigates

possibilities of controlling the motion of the bistable fronts by zero-mean ac forces.

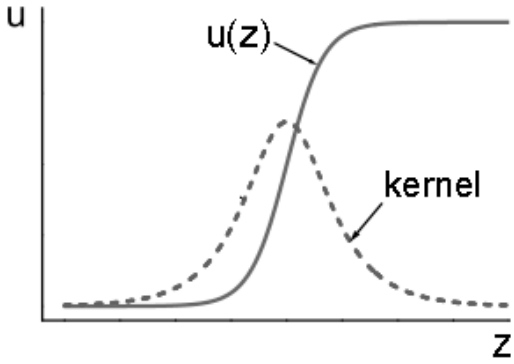

Figure 6. A traveling front solution $u(z)$ for reaction–diffusion equation connecting two equilibrium points

There is one more possible trajectory connecting saddle point u_1 with itself in the phase plane but this solution corresponds to the traveling pulse, which is not stable in regards to fluctuations.

It is worth to mention that front solution propagating in the opposite direction can be achieved by performing the transformation $u(z) = u(z,t)$, $z = x + ct$, where $c > 0$. If $u(z,c)$ is a solution, then $u(-z,-c)$ is also a solution. Indeed, the boundary conditions are required to change as well. Then similarly to the $u - v$ phase plane represented in Figure 5, the unique trajectory connecting saddle point $(u_1, 0)$ with $(u_3, 0)$ as t increases in the fourth quadrant of the $u - v$ plane corresponds to the traveling anti-front solution.

The next step after the existence of the traveling BFs is known – stability of the BF with regard to the small fluctuations.

2.2.2 Stability of Bistable Front

Stability of the BF may be proved by use of the perturbation theory that describes the particular case of the weakly perturbed system being only slightly deviated from its stationary "state" $u_0(z)$. The weak forcing $\varepsilon f(t)$ is added to the equation (5):

$$u_t + \hat{\Lambda} u = \varepsilon f(t),\ \varepsilon << 1. \tag{19}$$

Here the nonlinear operator $\hat{\Lambda}$ has the following form,

$$\hat{\Lambda} = -\ \frac{\partial^2}{\partial z^2} - c_0\ \frac{\partial}{\partial z} + R(u). \tag{20}$$

It follows that the front solution $u(z,t)$ is slightly deviated,

$$u(z,t) = u_0(z) + \Delta u(z,t), \tag{21}$$

where $\Delta u(z,t)$ denote the small deviation. Substituting (21) into (19) and applying the linearization procedure one rewrites the equation as follows:

$$\frac{\partial u_0}{\partial z}\frac{ds}{dt} + \frac{\partial \Delta u}{\partial t} + \hat{L}\Delta u = F(f; \Delta u, c, u_0), \tag{22}$$

Here the linear operator $\hat{L}$ is defined as follows:

$$\hat{L} = -\frac{d^2}{dz^2} - c_0\frac{d}{dz} + U(z), \tag{23}$$

and the associated potential $U(z)$ is a function of both the rate function $R(u)$ and the front solution $u_0(z)$:

$$U(z) = R'[u_0(z)], \tag{24}$$

with the prime denoting the derivative with respect to the "variable" u_0. In deriving (22) from (19) the following relationship has been taken into account:

$$\hat{\Lambda} u_0(z) = 0. \tag{25}$$

This relationship describes the free (unperturbed) front ($f(t) = 0$). In the case of a small perturbation we expand the quantities c, Δu and F in a power series of a small parameter β,

$$A_n = \sum_{n=1} \beta^n A^{(n)},\ A = c(t),\ \Delta u(z,t),\ F(z,t) \tag{26}$$

By substitution of the equation (26) into (22) the following evolution equation

may be obtained in the β^n order approximation,

$$\frac{\partial u_0}{\partial z}\frac{ds^{(n)}}{dt}+\frac{\partial \Delta u^{(n)}}{\partial t}+\hat{L}\Delta u^{(n)}=F^{(n)}, \tag{27}$$

This is the main equation in perturbation theory that connects to unknown functions, $s^{(n)}(t)$ and $\Delta u^{(n)}(z,t)$. Expanding the function $\Delta u^{(n)}$ and $F^{(n)}$ through the complete set of the eigenfunctions Y_α,

$$\begin{aligned}\Delta u^{(n)}(z,t)&=\sum_\alpha T_\alpha^{(n)}(t)\,Y_\alpha(z),\\ F^{(n)}(z,t)&=\sum_\alpha F_\alpha^{(n)}(t)\,Y_\alpha(z),\end{aligned} \tag{28}$$

one rewrites the equation (27) in the "L-representation" with T_α:

$$\frac{dT_\alpha^{(n)}(t)}{dt}+\lambda_\alpha T_\alpha^{(n)}=\left\langle Y_\alpha\middle|F^{(n)}(t,z)\right\rangle \tag{29}$$

where the introduced notation is expressed as follows:

$$\left\langle Y_\alpha\middle|F^{(n)}(t,z)\right\rangle:=\int_{-\infty}^{+\infty}dz\,Y_\alpha^{+}(z)\,F^{(n)}(t,z) \tag{30}$$

The evolution equations that describe the required function $T_\alpha^{(n)}$ may be simply obtained from the equation (29):

$$T_\alpha^{(n)}(t)=\int_0^t d\tau\,\exp[\lambda_\alpha(\tau-t)]\left\langle Y_\alpha(z)\middle|F^{(n)}(t,z)\right\rangle \tag{31}$$

The one can see that solutions $T_\alpha^{(n)}$ decay if $\lambda_\alpha>0$ – the solution $u_0(z)$ is stable because the small deviation $\Delta u(z,t)$ decays in time.

Now, we need to check if $u_0(z)$ is stable in the eigenvalues spectrum $\{\lambda_\alpha\}$. The following invariant "skeleton" equation is invariant for the translation, with respect to the infinity small translation δz:

$$u_{0zz}+c_0\,u_{0z}-R[u_0(z)]=0. \tag{32}$$

As follows, both $u_0(z)$ and $u_0(z+\delta z)$ are equally well solutions to the equation (32). Substituting $u_0(z+\delta z)=u_0(z)+u_0'(z)\,\delta z$ into the equation (32) one can see that function $u_0'(z)$ should satisfy the following linearized equation:

$$\hat{L}\,u_0'(z)=0. \tag{33}$$

It should be noted that linear operator $\hat{L}$ is the same as in the perturbation theory (23). So, the translational (Glodstone) mode $\overline{Y}(z)\equiv u_0'(z)$ corresponds to the eigenvalue $\overline{\lambda}=0$ of the operator $\hat{L}$:

$$\hat{L}\overline{Y}(z) = 0,\ \overline{Y}(z) = du_0(z)/dz \tag{34}$$

One can see that the function $\overline{Y}(z) \equiv u_0'(z)$ does not have zero points. As a result, the eigenvalue $\overline{\lambda} = 0$ is minimum and corresponds to the main "mode" of operator $\hat{L}$ (eigenfunction with minimal eigenvalue). Then the eigenvalue problem of the given front solution is expressed as follows:

$$\hat{L}Y_\alpha(z) = \lambda_\alpha Y_\alpha(z),\ \lambda_\alpha \geq 0 \tag{35}$$

In summary, all eiqenvalues are positive, except the value, corresponding to the translation mode $\overline{Y}(z) \equiv u_0'(z)$. Therefore, the fort solution is always stable for weak perturbations expect in case of translation mode ($\overline{\lambda} = 0$). In addition, it can be proved that the translation mode describes changes only in the velocity of the front-solution.

2.2.3 Velocity of Bistable Front

In order to evaluate the velocity c of the free (unperturbed) bistable front, the equation (9) is transformed to

$$v\frac{dv}{du} + c\,v - R(u) = 0, \tag{36}$$

where $v = \frac{du}{dz}$. Then the equation (36) is multiplied by du:

$$v\ dv + c_0 v(u)\ du - R(u)\ du = 0. \tag{37}$$

First term is eliminated from the equation (37) by integrating both sides of the equation along the trajectory Γ_2 in the $u - v$ phase plane (Figure 5):

$$\int_\Gamma v\ dv = 0. \tag{38}$$

Then the expression of the velocity reads as follows

$$c_0 = \frac{-\Delta W}{\Delta J_v}, \tag{39}$$

where

$$\Delta J_v = \int_{u_3}^{u_1} v(u)\ du. \tag{40}$$

The term ΔJ_v stands for the plot limited by the Γ trajectory in the $u - v$ phase plane and a potential $W(u)$ has a relationship with the $R(u)$ such that

$$R(u) = -\frac{dW}{du}. \tag{41}$$

In fact, the potential $W(u)$ of the BF can be illustrated using a mechanical analogy – Newton's equation for a particle of coordinate u and with mass m in the potential $V(u)$ with friction coefficient γ (Figure 7):

$$m\,\ddot{x} + \gamma\,\dot{x} + V'(x) = 0 \tag{42}$$

There is a unique friction coefficient in the mechanical analog that the mass particle starts at u_1 and comes to the rest at u_3. If function $R(u)$ is imbalanced ($u_1 = 0,\ u_2 = 0.6,\ u_3 = 1$), then the friction coefficient γ is positive $\gamma > 0$ because there should be some force to stop mass particle at u_3 (Figure 7). In case of $u_2 = 0.5$, the friction coefficient $\gamma = 0$ and this corresponds to the stationary BF with velocity $c = 0$ in equation (9). Similarly, when the friction coefficient γ is negative $\gamma < 0$ ($u_2 = 0.4$), the mass particle starts at u_1 and comes to the rest exactly at u_3 (Figure 7).

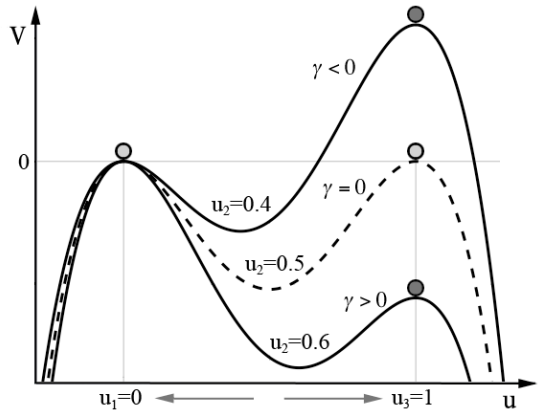

Figure 7. Potentials illustrate BF propagation in the mechanical analog for different unstable states u_2. Circles indicate mass particles in the potentials and maxima u_1 and u_3 indicate stable stationary solutions.

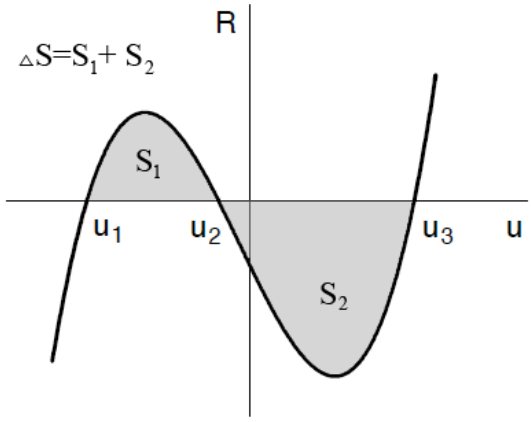

Figure 8. Illustration of the Maxwell's equal area rule. ΔS shows the area under the curve. Front moves backward if the area S_2 greater than S_1.

Another important aspect related to the velocity of the BF is Maxwell's equal area rule that describes a direction of free BF depending on the shape of the function $R(u)$ of N-type (Figure 8). Maxwell's construction is satisfied, *balanced* (the rate function $R(u)$ is *balanced*), when the plot ΔS limited by $R(u)$ function equals to zero:

$$\Delta S = \int_{u_3}^{u_1} R(u)\ du = 0. \tag{43}$$

The free (unperturbed) BF is static, motionless if Maxwell's construction is *balanced*, satisfied (ΔS=0). The direction of propagation of the BF depends on the dominating area. For example, the velocity will be negative, $c<0$, if the area S_2 being connected to u_3 is larger than the area S_1 and $\Delta J_v>0$ (Figure 8). In general, if the plot limited by trajectory Γ in $u-v$ phase plane is $\Delta J_v>0$, then Maxwell rule can be summarized as follows:

$$c\begin{cases}>0, & \Delta S>0\\ =0, & \Delta S=0\\ <0, & \Delta S<0\end{cases}. \tag{44}$$

2.2.4 Symmetry properties of the rate function

The ratchet-like transport of the BF depends on different symmetry families (classes) of the "similarly shaped" rate function $R(u)$ of N-type: symmetrical (symmetrically shaped) and asymmetrical (asymmetrically shaped) rate functions [15]. Class of the *self-similar* rate function of N-type is expressed as follows:

$$R(u;\ C)=R_0(u)+C, \tag{45}$$

where C is the free constant. It is possible to make the rate function $R(u;\ C)$, either symmetrical or asymmetrical one, to be *balanced* (Maxwell's construction is satisfied) by tuning values of the free constant C. If the balanced rate function $R(u)$ satisfies equality

$$R(u-u_2)=-R(u+u_2), \tag{46}$$

then the rate function is symmetrical (symmetrically shaped). By tuning values of the free constant C from the equation (45) one can arrive to different symmetrical (symmetrically shaped) rate functions as shown in Figure 9.

In contrast, the family of the rate functions $R(u;\ C)$ is asymmetrical (asymmetrically shaped), if the inequality holds

$$R(u-u_2)\neq -R(u+u_2). \tag{47}$$

Family of similarly shaped asymmetrical rate functions can be achieved by tuning values of the free constant C from the equation (45) (Figure 10).

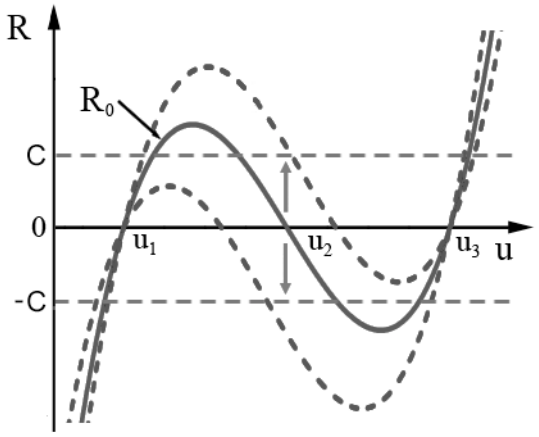

Figure 9. Illustration of family (class) of the symmetrical rate functions. Different similarly shaped symmetrical rate functions can be constructed by adjusting value of the free constant C.

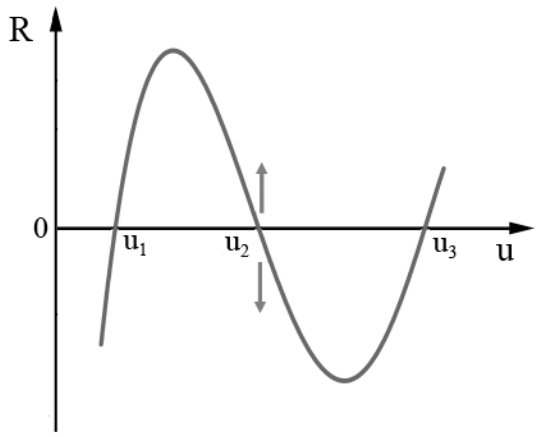

Figure 10. The same as in Figure 9 but for family (class) of the asymmetrical rate functions. The Maxwell's construction is balanced but the rate function is asymmetrical.

It is important to distinguish two families of symmetrical and asymmetrical rate functions because characteristics of the ratchet effect radically differ [15]. Assume that external symmetrical forcing f of zero mean with amplitude f_0 is acting on the bistable front. In case of family of the symmetrical rate functions, typical average $v - f_0$ characteristics that describe the dependence of the mean drift velocity, $v = \langle c \rangle$, of the ac driven BF versus the amplitude f_a of the symmetrical oscillatory force are presented in Figure 11. As one can see, when the Maxwell's construction is balanced, then it is impossible to accelerate (on average) motionless BF, witch stays initially at rest $c_0 = 0$. If Maxwell's construction is imbalanced (initially BF moves at some velocity, $c_0 \neq 0$), then the velocity of the BF only increases or decreases depending on the initial conditions [2].

Different situation when family of asymmetrically shaped rate functions are applied. The average $v - f_0$ characteristics presented in Figure 12. They could be typified as follows: the progressive dc motion of the static BF (curve B), the *reversal behavior* (changing direction) of the traveling BF (curve C), the directed net motion of the self-ordered BF is stopped (curve D). Other 3 curves (A, E, F) very similar to the case of symmetrically shaped rate functions (see detailed analysis in [15, 57]).

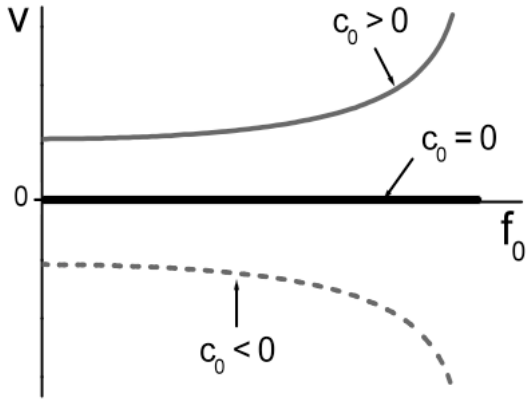

Figure 11. The mean drift velocity of the ac driven BF versus the amplitude of the symmetrical harmonic force in case of symmetrically shaped rate functions. The curves show the $v - f_0$ dependences being derived at different initial velocity of the free, undertreated BF.

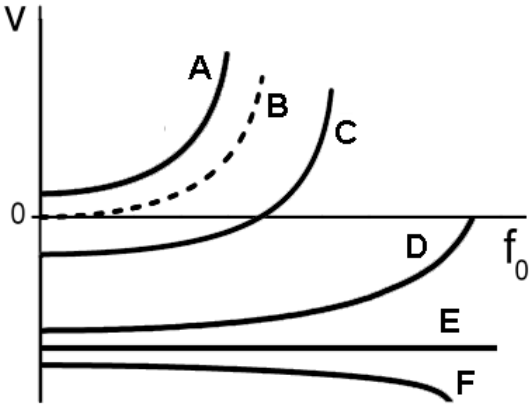

Figure 12 The same as in Figure 11 but for the family of the asymmetrical rate functions. Curves A, E, F acting similarly to curves in Figure 11. Curve B shows acceleration of motionless BF, curve C demonstrates reversal effect when BF changes direction. Finally, curve D shows stopping effect of the traveling BF.

It is impossible to construct asymmetrically shaped rate functions using sine-Gordon [3], cubic polynomial [4] models for witch analytic solution are known. Therefore, a "pseudolinear" model that is characterized by the piecewise-linear rate function $R(u)$ is considered in the present research. The piecewise-linear approximation exhibits the most important features of the bistable system and provides a model of the "flexible" symmetry that is analytically solvable [5].

2.2.5 Piecewise-linear rate function

The approximation of the rate function by the piecewise linear dependence can be expressed as follows:

$$R(u) = \begin{cases} \alpha_1(u - u_1), & u < u_M \\ -\alpha_2(u - u_2), & u_M < u < u_m \\ \alpha_3(u - u_3), & u > u_m \end{cases}, \tag{48}$$

where the rate function $R(u)$ has three zeroes at $u = u_1, u_2, u_3$ with the following relations: $R'(u_{1,3}) > 0$ and $R'(u_2) < 0$, where the prime denotes the derivative (Figure 13). The adjustable parameters α_i and u_i satisfy the relations: $u_1 < u_M < u_2 < u_m < u_3$ and $\alpha_i > 0$ ($i = 1, 2, 3$), where α_i is the slope coefficients of the rate function.

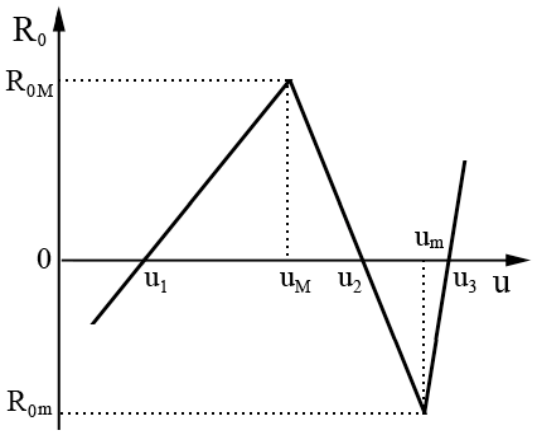

Figure 13. The piecewise-linear rate function with free zeroes at u_1, u_2 and u_3. Extreme maximum and minimum values are pointed by u_M and u_m, respectively.

The piecewise linear rate function used (a) is analytically tractable; both the free front solutions of BFs derivable by use of equation (5) and the perturbed ones, within the adiabatic approximation, are known explicitly [5, 15], (b) is of the flexible $R(u)$ symmetry; by taking $\alpha_1 = \alpha_3$ and $\alpha_1 \neq \alpha_3$ one arrives at both cases of the symmetrical and asymmetrical rate functions, respectively, (c) reproduces qualitatively well enough the characteristic features of the bistable system; both the speed functions $c(t)$ and the average characteristics of the spurious drift of BFs derivable by use of both the prototype (cubic polynomial (7)) rate function and its piecewise linear emulations (48) satisfying the same $R(u)$ symmetry are very close to each other, as shown in [17, 57]. Therefore, the pseudolinear model is a sufficient tool to investigate ratchet-like transport.

It is useful to introduce new parameters in order to control balance of the rate function $R(u)$. The maximum $R_M \equiv R(u_M)$ and minimum $R_m \equiv R(u_m)$ extreme values of the rate function $R(u)$ can be expressed as

$$R_M = \alpha_2(u_2 - u_M) \text{ and } R_m = \alpha_2(u_2 - u_m). \tag{49}$$

The balance parameter h_R of the rate function is defined by the relation

$$h_R = -\frac{R_M}{R_m}. \tag{50}$$

It follows that by tuning the balanced parameter h_R one can get different propagation rates c_0 of the free, unperturbed ($f(t) = 0$) BF. If the Maxwell's construction of the rate function is balanced, then the free BF is static ($c_0 = 0$) and the equality $h_R = h_0$ holds, where

$$h_0 = \sqrt{\frac{(1+r_3^{-1})}{(1+r_1^{-1})}}. \tag{51}$$

The slope parameters of the rate function are expressed as $r_{1,3} = \alpha_{1,3}/\alpha_2$. On the other hand, if the rate function is unbalanced ($h_R \neq h_0$), then the free BF travels at the constant velocity ($c_0 \neq 0$). It is convenient to set unbalanced rate function using parameter g_H in the expression $h_R = g_H h_0$. The maximal propagation rate $c_0 \to c_M$ is achieved by taking the limit $h_R \to \infty$, where $c_M = 2\sqrt{\alpha_2}$ is the marginal velocity of BF [15]. In contrast, the free BF moves backward ($c_0 \to -c_M$), if $h_R \to 0$.

The scaled speed functions $s(t)$ being defined by the relation $s(t) = c(t)/c_M$ are preferable over the ordinary (non-scaled) ones. The scaled velocity of the driven BF $s(t)$ satisfies the relation $s(t) \in (-1, 1)$, regardless to the balanced parameter value h_R used [17, 57]. Quite similarly, the scaled velocity of the free, unperturbed BF, $s_0 = c_0/c_M$, takes values within the interval $(-1, 1)$, more specifically, the following relations hold: $s_0 \to 1$ if $h_R \to \infty$ and $s_0 \to 0$ if $h_R \to 0$. As a result, the scaled speed functions $s(t)$ are the central subject of the present research that is calculated using numerical methods.

It is worth to mention, the both heights, $\Delta R = R_M(u_M;\, C) - R_m(u_m;\, C)$, of self-similar rate functions $R(u;\, C)$ and the positions of the extremes, being located at $u = u_M$ and $u = u_m$ do not depend on the free constant C. Therefore, from the equation (48), if used in conjunction with (45), follows that

$$R_M = h_R(1+h_R)^{-1}\Delta R,\; R_m = -(1+h_R)^{-1}\Delta R, \tag{52}$$

and the zero-points of the rate function are described by the expressions,

$$\begin{aligned} u_1 &= u_M - \alpha_1^{-1} R_M, \\ u_2 &= u_M - \alpha_2^{-1} R_M, \\ u_3 &= u_m - \alpha_3^{-1} R_m. \end{aligned} \tag{53}$$

Control of the front-structures by symmetrical and asymmetrical rate functions, described by the linear pieces (Figure 13), has been studied in the extensive literature analytically and by numerical simulations [15, 16, 58, 59].

2.2.6 Analytical solution of pseudolinear model

Without giving the details of the calculations, which are straightforward albeit lengthy, analytical front solutions of the free BF (5) using pseudolinear model (48) can be expressed as follow (for details see [5]):

$$u(z)=\begin{cases} u_1+(u_M-u_1)\exp(k_1 z),\ z<0 \\ u_2+(u_2-u_M)b(w)\exp(-wz)\sin(q_2 z-\Psi),\ 0<z<z_m \\ u_3-(u_3-u_m)\exp[k_3(z-z_m)],\ z>z_m . \end{cases} \quad (54)$$

For the sake of brevity the abbreviation $w=c(t)/2$ have been introduced. The required parameters are described as follows:

$$\begin{aligned} &k_{1,3}(w)=-w\pm\sqrt{w^2+\alpha_{1,3}},\ q_2(w)=\sqrt{\alpha_2-w^2}, \\ &b(w)=\{1+1/\theta^2(w)\}^{1/2},\ \theta(w;\ \delta_1)=\frac{q_2(w)}{g_2(w)}, \\ &\Psi=\begin{cases}\arctan[\theta(w)],\ \theta(w)>0 \\ \pi-\arctan[-\theta(w)],\ \theta(w)<0,\end{cases} \\ &z_m=q_2^{-1}\Phi(w;\alpha_1,\alpha_3) \end{aligned} \quad (55)$$

The auxiliary functions are given by the expressions

$$\begin{aligned} &g_{1,3}(w)=-w+\delta_{1,3}k_{1,3}(w), \\ &\Phi(w)=\begin{cases}\arctan[Tg(w)],\ Tg(w)>0 \\ \pi-\arctan[-Tg(w)],\ Tg(w)<0,\end{cases} \end{aligned} \quad (56)$$

where

$$\begin{aligned} &Tg(w)=f_{Sn}/f_{Cn},\ f_{Sn}=q_2(w)[\delta_1 k_1(w)-\delta_3 k_3(w)], \\ &Sn(w)=f_{Sn}/f_V,\ f_{Cn}=-[q_2^2(w)+g_1(w)g_3(w)], \\ &Cn(w)=f_{Cn}/f_V,\ f_V=q_2^2(w)+q_1^2(w). \end{aligned} \quad (57)$$

Here the following denotations have been introduced; $\delta_i=\alpha_2/\alpha_i$ and $j_i=1+\delta_i$.

3. Spatio-temporal control of Bistable Front

The focus of this research is to study spatio-temporal control of the directed net motion of the self-ordered fronts by the oscillatory force of zero-time average, either noisy or regular one, with a help of computer modeling. Therefore, the directly induced dc motion, namely, the ratchet-like transport derivable by the additive zero-average force acting on the BF is studied in this chapter. Important to emphasize that the directly induced dc drift implies that the average force $f(t)$ acting on the front in the system equals zero. In mathematical terms the governing equation of the directly driven BF may be represented by the following PDE of parabolic type:

$$u_t - u_{zz} - c\,(t)u_z + R(u) = f(t) \tag{58}$$

where $f(t)$ denotes oscillatory force acting on the front in the system. The mechanism of the "speed rectification" implies the oscillatory force $f(t)$ of zero-time average is converted into the speed function $c(t)$ of a finite time average was discussed in [17]. Broadly speaking, the "speed rectification" is a nonlinear transformation process, which converts the oscillatory "input" function $f(t)$ of zero-time average into the "output" (response) function $c(t)$ of a finite time average. The spurious drift dc of the bistable front depends on the temporal symmetry of the ac force $f(t)$ acting on the front in the system [17, 58, 60]. It was shown in [15, 16, 18] that results derivable using different "symmetry" of the forcing functions radically differ. To summarize, the unforced dc drift of the self-ordered fronts usually originates due to the "hidden" asymmetry of the system or it comes from the broken temporal symmetry of the oscillatory force acting on the front in the system. Consequently, the symmetry properties of both $R-u$ and $f-t$ dependences play a prominent role in controlling the ratchet-like transport of BFs.

Nevertheless, the noise-induced drift of BFs under temporally irregular ac forces remains still insufficiently explored because it has been studied by use of the perturbation techniques, by assuming the stochastic force to be weak [10, 12, 13]. The ratchet-like transport being investigated within the cubic

polynomial (7) and sine-Gordon (8) models demonstrated that the noise-induced dc drift of BFs under the weak, low-intensity noisy forces was sensitive to the spectral content of the forcing (noise spectrum). It is important to note that the white (uncorrelated) Gaussian noise is not capable to induce the directed net motion of the BF as it was shown in [12]. In other words, the noise-induced drift of BFs under weak noisy forces disappears in both cases of the symmetrical and asymmetrical rate functions if the noisy force is Gaussian and delta correlated [10, 11, 13]. The results derivable within the perturbation theory are of limited use. Therefore, there is a need to use other methods like computer modeling to investigate the ratchet-like transport at the higher levels of the noise, beyond the perturbative approaches discussed.

The present chapter is organized as follows. In the beginning the oscillatory forcing functions used in this research to analyze the ratchet-like transport of BFs are presented. Later, the perturbation theory and adiabatic approximation are discussed in order to find the characteristic relaxation time of the system and the speed function of the quasi-stationary driven BFs, respectively. Finally, computer modeling of the problem (58) is described in the last sections.

3.1 Forcing functions

As discussed, the ratchet-like transport of BFs is sensitive to the peculiarities (shape) of the oscillatory forcing function $f(t)$. Zero-mean force is treated as time-symmetric (contrasymmetric) if the equality $f(t+T/2)=-f(t)$ holds, where by T we denote the period of the ac force. Differently, zero-mean force $f(t)$ is time-asymmetric if the relation $f(t+T/2)\neq -f(t)$ holds. The spurious drift of BF, more specifically, the shift of the mean drift velocity of the ac driven BF, derivable by both the time-symmetric (symmetrically shaped) and time-asymmetric (symmetrically shaped) forcing functions notably differ [15, 16, 18]. We shall deal with the multi-harmonic forcing functions $f(t)$ that may be presented by superposition of the single-harmonic components (Fourier modes). The shape of the multi-harmonic function $f(t)$ is controllable by varying the spectral content, the

relative phases and the amplitude-to-frequency ratios of the harmonic modes. This provides a convenient method of controlling the "efficiency" of the multi-harmonic ac driver, in terms of the spurious drift discussed. The "efficiency" of ac driver may be evaluated by use of the acceleration factor, $\rho := |s_0|^{-1} v$, denoting the relative increase of the mean drift velocity, $v = \langle s(t) \rangle$, of the ac driven of BF.

3.1.1 Single-harmonic forcing function

The time-symmetric forcing function is used to investigate the influence of the time lags on the ratchet-like transport of BFs drivable by the asymmetrical rate functions (48). The focus is on the role of $R - u$ symmetry in the dynamics of the rectified oscillatory motion of BFs, namely, the response of BF to the single-harmonic forcing function is considered,

$$f(t) = f_0 \sin(\omega t). \tag{59}$$

Moreover, the forcing function (59) is of the "highest" temporal symmetry: it satisfies the time-shift relation, $f(t + T/2) = -f(t)$, and time-inversion symmetry relation, $f(t_N - t) = -f(t_N + t)$, where the notation t_N stands for the N-th zero-point of the oscillatory function $f(t)$, namely, one has that $t_N = 2N\pi$ where $N = 0, \pm 1, \pm 2, \ldots$ Clearly, the amplitude f_0 of the oscillatory force acting on the front cannot exceed the critical value, $f_{Mx} = \min\{R_M, -R_m\}$, above which the global stability of the ac driven BF breaks down. Thus, we shall demand in what follows that $f_0 < f_{Mx}$.

3.1.2 Bi-harmonic forcing function

In order to investigated the influence of temporally irregular oscillations (fluctuations) of the unbiased oscillatory forcing on the spurious drift of BFs, the bi-harmonic forcing functions being a superposition of the single-harmonic components (Fourier modes) of the different frequencies, either commensurate or incommensurable ones, are used. The bi-harmonic forcing functions exhibit the temporally irregular behavior and are used to study the "efficiency" of the ac driver, either periodic or quasi-periodic. The bi-harmonic function is

described by the following expression:

$$f(t) = f_0(1+b_F)^{-1}\left[\sin(\omega\, t) + b_F \sin(\mu\, \omega\, t + \Delta\varphi)\right] \tag{60}$$

where b_F, μ, $\Delta\varphi$, and f_0 stand for the free, adjustable parameters. By taking the free parameter μ to be the rational/irrational number one arrives at the periodic/quasi-periodic forcing functions below labeled by $f_P(t)$ and $f_Q(t)$, respectively. In order to evaluate the effect of the temporally irregular oscillations of the quasi-periodic forcing on the performance of the ratchet-like shuttling of BFs, the characteristic parameters of both oscillatory functions $f_P(t)$ and $f_Q(t)$ must be properly chosen. To be more specific, the frequencies and the amplitude-to-frequency ratios of the single-harmonic components of both forcing functions $f_P(t)$ and $f_Q(t)$ should be close to each other. Namely, the parameter values $\mu = 2$ and $\mu = \sqrt{3}$ are taken to obtain the periodic and quasi-periodic forcing functions, $f_P(t)$ and $f_Q(t)$, respectively. Moreover, the adjustable parameters are as follows: $b_F = 1$ and $\Delta\varphi = \pi$. Another important parameter of the ac driver is the amplitude (maximal deviation) f_a of the oscillatory force $f(t)$. The amplitude f_a can be expressed for the quasi-periodic forcing functions discussed $f_Q(t)$ as follows:

$$f_a = f_0. \tag{61}$$

To find amplitude f_a for periodic forcing functions $f_P(t)$, we need to substitute parameters $\mu = 2$, $b_F = 1$ and $\Delta\varphi = \pi$ into equation (60):

$$f = \frac{f_0}{2}\left[\sin\omega\, t + \sin(2\,\omega\, t + \pi)\right] = \frac{f_0}{2}\sin\omega\, t\,(1 - 2\cos\omega\, t). \tag{62}$$

By substituting $x = \omega\, t$ into (62) we look for extreme values:

$$\begin{gathered} f' = \frac{f_0}{2}(\cos x - 2\cos 2x) = 0 \\ \downarrow \\ 4\cos^2 x - \cos x - 2 = 0. \end{gathered} \tag{63}$$

By substituting $y = \cos x$ into (63) one gets the following equation with vertexes:

$$4\,y^2 - y - 2 = 0,$$
$$y_{1,2} = \frac{1}{8} \pm \sqrt{\frac{1}{64} + \frac{1}{2}} \equiv \frac{1 \pm \sqrt{33}}{8}. \quad (64)$$

By substituting $\cos_{1,2} x = \frac{1 \pm \sqrt{33}}{8}$ into (62) of the form

$$f(t) = \frac{f_0}{2} \sin x\,(1 - 2\cos x) \equiv \pm \frac{f_0}{2} \sqrt{1 - \cos^2 x}\,(1 - 2\cos x), \quad (65)$$

one can arrive to the expression of the amplitude f_a of the periodic forcing function $f_P(t)$:

$$f_a = \frac{f_0}{64}(30 + 2\sqrt{33})^{1/2}(3 + \sqrt{33}) \approx 0.88 f_0. \quad (66)$$

Clearly, the amplitude f_a of the oscillatory force acting on the front cannot exceed the critical value, $f_{Mx} = \min\{R_M, -R_m\}$, above which the global stability of the ac driven BF breaks down. The relation $f_a < f_{Mx}$ should be satisfied. For comparison, both forcing functions $f_P(t)$ and $f_Q(t)$ are depicted in Figure 14.

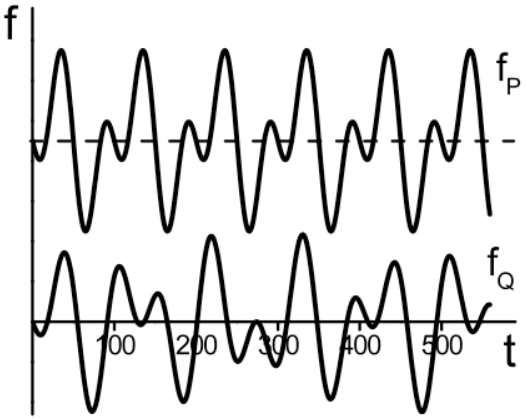

Figure 14. The periodic (f_P) and quasi-periodic (f_Q) forcing functions. The period of the basic mode of both oscillatory functions was taken as follows: T = 100.

Finally, the quasi-periodic forcing functions that involve the mixed-mode oscillations with two incommensurable frequencies (bi-harmonic functions) have been used to study the directed transport of the point-particles [61, 62].

3.1.3 Multi-harmonic forcing function

The spatio-temporal control of the quasi-periodically forced BFs is investigated further approximating the oscillatory force $f(t)$ by the multi-harmonic forcing function being a linear combination (sum) of the single-

harmonic components with the incommensurate, rationally independent frequencies. The multi-harmonic oscillatory forces $f(t)$ that are characterized by the incommensurate "frequency mixing" of the single-harmonic components exhibit the temporally irregular behavior. By gradually extending the frequency spectrum of the oscillatory force we investigate whether and how noticeable the deterministic, temporally irregular ac forces of the different spectral content are capable to support the directed net motion of the ac driven front. The quasi-periodic ac forces discussed that involve the mixed-mode oscillations with the greatly differing amplitudes exhibit a similarly looking behavior to the noisy ones; they may be treated as the deterministic "equivalent" (emulation) of the noisy forces. As it was shown in [63, 64], the stochastic, randomly oscillating function may be presented by a superposition of the single-harmonic components (harmonic modes) that are characterized by the randomly distributed frequencies, both the commensurate and incommensurate ones. In particular, the Gaussian random function of zero mean and delta correlated is characterized by the infinitely broad frequency spectrum of the harmonic modes. The multi-harmonic forcing function can be expressed as follows,

$$f(t) = f_a \, A_F \left[\sin(\omega \, t) + \sum_{j=1}^{N} b_j \sin(\mu_j \, \omega \, t + \Delta\varphi_j) \right] \qquad (67)$$

where f_a, b_j, μ_j and $\Delta\varphi_j$ denote the free, adjustable parameters. In addition, the notation ω stands for the frequency of the fundamental mode of the ac forcing and N is an integer. The bi-, tri-, tetra-, and penta-harmonic forcing functions derivable by gradually increasing the integer value N ($N = 1, 2, 3, 4$) in expression (67) are investigated. The multi-harmonic function (67) implies the constructive/destructive superposition of the separate modes takes place: The auxiliary parameter A_F derivable numerically equalizes ("normalizes") the amplitudes f_a of the separate forcing functions $f(t)$ being derived at the different number N of harmonic modes. More specifically, the parameter A_F is a function of the parameters $\Delta\varphi_j$, ω_j, and N. The free parameter μ_j is used to

make the periodic, $f_P(t)$, and quasi-periodic, $f_Q(t)$, forcing functions by taking rational and irrational numbers, respectively. Obviously, the frequencies and the amplitude-to-frequency ratios of the single-harmonic components of both forcing functions $f_P(t)$ and $f_Q(t)$ should be close to each other. Namely, the frequencies, $\omega_j = \mu_j \omega$, and the amplitude-to-frequency ratios b_j/ω_j of the single-harmonic components of both oscillatory functions $f_P(t)$ and $f_Q(t)$ should be taken close to each other. In other words, the expressions $\mu_{Pj} \approx \mu_{Qj}$ and $b_{Pj} = b_{Qj} = 1$ should be satisfied. The characteristic parameters of the forcing functions used, $f_P(t)$ and $f_Q(t)$, are presented in Table 1.

	N	1	2	3	4
$f_Q(t)$	μ_{Qj}	$\sqrt{3} \approx 1.73$	$\pi \approx 3.14$	$\pi\sqrt{2} \approx 4.44$	$e\sqrt{3} \approx 4.71$
$f_P(t)$	μ_{Pj}	2	3	4	5

Table 1. The characteristic parameters of the forcing functions used.

In addition, considering the ratchet-like shuttling of BFs the temporal symmetry of the oscillatory force $f(t)$, namely, the symmetry of $f-t$ dependence with respect to the *t*-axis, plays a relevant role. Broadly speaking, the function $f(t)$ is time-symmetric if the relation $\max\{f(t)\} = -\min\{f(t)\}$ holds and time-asymmetric if the inequality $\max\{f(t)\} \neq -\min\{f(t)\}$ holds [16, 17]. More specifically, the periodic functions $f_P(t)$ are time-asymmetric if one takes that $\Delta\varphi_j = \pi$ [16]. The temporal oscillations of the quasi-periodic functions $f_Q(t)$ are, loosely speaking, symmetrically shaped "on average", i.e., the spurious drift of the quasi-periodically forced BFs derivable by the rigorously symmetric rate functions disappears asymptotically, in the limit $t \to \infty$ [61, 62]. The multi-harmonic forcing functions $f_P(t)$ and $f_Q(t)$ are depicted in Figure 15 and Figure 16, respectively.

Finally, the amplitude (maximal deviation) f_a of the oscillatory force $f(t)$ should satisfy the global stability relation $f_a < f_{Mx} = \min\{R_M, -R_m\}$.

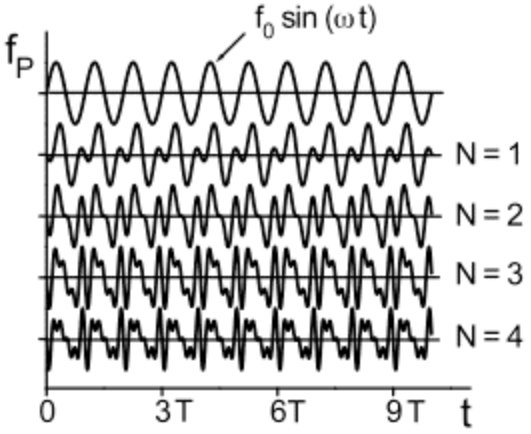

Figure 15. The periodic (f_P) forcing functions: the bi- (N = 1), tri- (N = 2), tetra- (N = 3), and penta-harmonic (N = 4) functions, as follows from equation (67). The period of the basic mode of all oscillatory functions was taken as follows: $T = 10$.

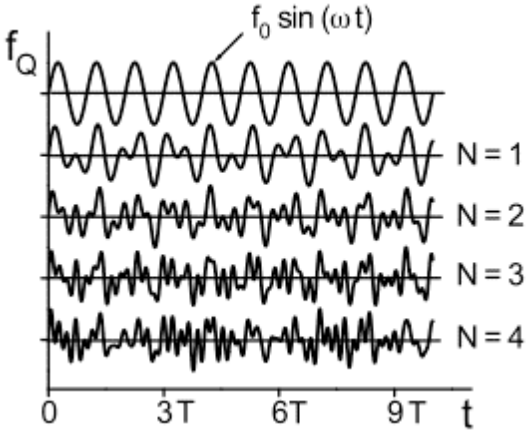

Figure 16. The same as in Figure 15, but for the other case of the quasi-periodic (f_Q) forcing functions that exhibiting the temporally irregular behavior.

3.1.4 Bounded noise forcing function

In this section we continue investigate how different spectral content is capable to support the directed net motion of the ac driven front using bounded noise forcing. Bounded noise is chosen because the multi-harmonic forcing function (67) only exhibits temporally irregular behavior but it is not a noise. In general, a random force may be presented by a superposition of the single-harmonic modes being characterized by the randomly distributed frequencies [63, 64]. Bounded noise is a multi-harmonic function with constant amplitude and random frequency and phases. In addition, it is used to investigate various systems and, in case of ratchet effect, it is interesting to research what happens with the BF under bounded noise by gradually extending the frequency spectrum of the bounded noise. The direct calculations being performed within both the sine-Gordon models of the system, by use of the perturbation techniques demonstrated that a white Gaussian noise was not capable to induce the directed net motion of BF [12]. Bounded noise functions may be constructed using a combination of large number N of Fourier modes, as follows:

$$f(t) = f_0 \frac{1}{N} \sum_{n=1}^{N} \sin(\omega_n \, t + \varphi_n) \, \Theta(\omega_M - \omega_n) \tag{68}$$

where random variables ω_n and φ_n are the frequency and phase, respectively, and they are uniformly distributed in the following intervals: $\omega_n \in [\omega_m, \omega_M]$ and $\varphi_n \in [0, 2\pi]$; the subscripts m and M denote "minimal" and "Maximal", respectively. The theta function Θ is used to bound spectral content in the forcing function (68). The intensity of the stochastic function (68) we define using standard deviation σ:

$$\sigma^2 \equiv \left\langle f^2(t) \right\rangle = \lim \frac{1}{\Delta T} \int_0^{\Delta T} dt \, f^2(t), \text{ when } \Delta T \to \infty. \tag{69}$$

Here ΔT is a time period while the force acting on the BF. By substituting (68) into (69) one gets that:

$$\sigma^2 = \frac{f_0}{N} \frac{1}{\Delta T} \int_0^{\Delta T} dt \left\{ \sum_{n=1}^{N} \sin(\omega_n \, t + \varphi_n) \, \Theta(\omega_M - \omega_n) \right\}, \quad \Delta T \to \infty. \tag{70}$$

In order to ensure that the average force $f(t)$ acting on the front in the system equals zero, $< f(t) >= 0$, the time period long enough:

$$\Delta T >> \frac{2\pi}{\omega_m}. \tag{71}$$

Here ω_m stands for the period of the slowest mode of the forcing function (68).

Another important issue is to find the maximal value of the deviation σ_{Max} of the applied force (68) above which the front is not stable anymore. Stability criterion $f_a < f_{Mx} = \min\{R_M, -R_m\}$, used with other forcing functions, is not suitable because of the retardation effects (described in the next section). The maximal deviation σ_{Max} can be found numerically using equation

$$u_t + R(u) = f(t) \tag{72}$$

with the initial values $u_1(t=0) = u_{01}$ and $u_1(t=0) = u_{01}$, where u_{01} and u_{03} are the outer zero-points of the rate function (48). To be more specific, solving the equation (72) one has to gradually increase value of the amplitude f_0 in the forcing function (68) until the following stability criterions are satisfied: $R[u_1(t)] < R_M$ and $R[u_3(t)] < R_m$. Here the maximum $R_M \equiv R(u_M)$ and minimum

$R_m \equiv R(u_m)$ extreme values of the rate function (48) are calculated using the expressions (49). The standard deviation should satisfy inequality, $\sigma < \sigma_{Max}$, above which the global stability of the ac driven BF may break down.

Numerically found characteristics $\rho - \sigma$ of the spurious drift of BFs derivable by the bounded noise forcing functions (68) with the same parameters deviate from each other because of the random frequency and phases. For this reason the characteristics $\rho - \sigma$ have to be averaged:

$$\langle \rho - \sigma \rangle_r = \frac{1}{r} \sum_{i=1}^{r} \rho_i - \sigma_i . \tag{73}$$

Numerical simulations have showed that gradually increasing parameter r average characteristics $\rho - \sigma$ coincide within the accuracy of few tenths of percent. Therefore, in order to find the average characteristics $\rho - \sigma$, r realizations of forcing functions (68) have to be generated (optimal value $r = 20$). Additionally, the distribution density γ_ω in the frequency spectrum $[\omega_m, \omega_M]$ is constant for all realizations of the forcing functions with different parameters:

$$\gamma_\omega \equiv \frac{N}{\omega_M - \omega_m} = const . \tag{74}$$

3.2 Analytic tools

The governing equation (58) is not solvable analytically. In view of this, the purpose of this section is to describe the analytic tools for special cases: perturbation theory to find the characteristic relaxation time and adiabatic approximation to find the front solution of the slowly driven BF.

3.2.1 Perturbation theory

The characteristic relaxation time of the system, τ_R, which describes the rate of the transient processes in the system is analytically not obtainable (e.g., see [59], [11]); the analytical techniques of finding the front-solutions of the ac driven BF are lacking. Numerical methods can be used to find parameter τ_R in

case of strongly perturbed system. Nevertheless, a rough estimate of the required parameter τ_R may be obtained by use of the perturbation theory that describes the particular case of the weakly perturbed system being only slightly deviated from its stationary "state" $u_0(z)$. If the forcing function $f(t)$ is replaced by the weak forcing $\varepsilon f(t,z)$, where $\varepsilon << 1$, then the solution of equation (58) $u(z,t)$ and instantaneous velocity $c(t)$ may be presented in the following way,

$$u(z,t) = u_0(z) + \Delta u(z,t) \text{ and } c(t) = c_0 + \Delta c(t), \quad (75)$$

where $\Delta u(z,t)$ and $\Delta c(t)$ denote small deviations. The temporal behavior of the system being only slightly deviated from its stationary state $u_0(z)$ is obtainable through the linearization procedure of the governing equation (58) with the rate function (48) given by [2, 11, 18, 54]

$$\Delta u_t(z;t) + \hat{L}\Delta u(z;t) - \Delta c(t)u_{0z} = f(t,z) + O[\Delta u, \Delta c; u_0(z)], \quad (76)$$

where the auxiliary function $O(z,t)$ involves the nonlinear terms in Δu and Δc. The equation (76) holds in any case of the weak forcing $\varepsilon f(t,z)$, either noisy or regular one, which produces small deviations Δu and Δc. In addition, the linear operator $\hat{L}$ is defined as follows:

$$\hat{L} = -\partial_{zz} - c_0\partial_z + U(z). \quad (77)$$

Here the associated potential $U(z)$ is a function of both the rate function $R(u)$ and the front solution $u_0(z)$:

$$U(z) = R'[u_0(z)], \quad (78)$$

with the prime denoting the derivative with respect to the "variable" u_0. As it follows from equation (76), the temporal behavior of the weakly perturbed system may be evaluated by solving the following eigenvalue problem:

$$\hat{L}Y_\alpha(z) = \lambda_\alpha Y_\alpha(z), \quad (79)$$

where the notations Y_α and λ_α stand for the eigenfunction and the corresponding eigenvalue of the linear operator $\hat{L}$, respectively. An ordered set of the eigenvalues λ_0 denoting the characteristic relaxation rates (exponents), $\tau_\alpha^{-1} = \lambda_\alpha$, of a weakly perturbed system is called spectrum of eigenvalues $\{\lambda_0\}$ and depends on the peculiarities of the potential $U(z)$ (78). Thus, the potential

function $U(z)$ describes the potential well with two maxima being at infinity, $z \to \pm\infty$, and the minimum being located at the point $z = z_m$. In case of the pseudolinear rate function (48), relations that are followed directly from equation (78) holds: $U_{-\infty} = a_1$, $U_{+\infty} = a_3$ and $U(z_m) = -a_2$ (Figure 17). The eigenvalues spectrum $\{\lambda_0\}$ contains at least one discrete (separate) eigenlevel, $\lambda^- = 0$, being related to the translational (Glodstone) mode, $\overline{Y}(z) \propto u_0'(z)$, and the continuous spectrum of the eigenvalues λ_k being separated from the discrete eigenlevel $\overline{\lambda}$ by the gap $\Delta\lambda$, which depends on the peculiarities of the potential function $U(z)$. As one can see in Figure 17, the relation $\Delta\lambda = \lambda_{\min} - \overline{\lambda} \equiv \lambda_{\min}$ holds, where the bottom of the continuous spectrum $\lambda_{\min} \le \lambda_k$ can be expressed as follows $\lambda_{\min} = \min\{R'(u_1), R'(u_3)\}$. In addition, $\overline{\lambda}$ is the minimal eigenvalue of the spectrum $\{\lambda_0\}$ and the rigorous equality $\overline{\lambda} \equiv \min\{\lambda_\alpha\} = 0$ is satisfied in any case of the front solution $u_0(z)$ joining two steady states of the bistable system. Consequently, the equality $\Delta\lambda = \lambda_{\min} = \min\{\alpha_1, \alpha_3\}$ holds in case of the pseudolinear rate function (48). Finally, the slowly developing processes play a prominent role in considering low relaxation rates τ_α^{-1}. The characteristic (largest) relaxation time τ_R of the "pseudolinear" system being only slightly deviated from its stationary state $u_0(z)$ can be expressed follows:

$$\tau_R = \max\{\alpha_1^{-1}, \alpha_3^{-1}\}. \tag{80}$$

As the given estimate (80) suggests, by tuning the outer slope coefficient, either α_1 or α_3, one lengthens or shortens the time duration τ_R, namely, the different rates of the transient processes in a weakly perturbed system can be achieved. Finally, it is not clear enough whether the equality (80) holds in case of strongly perturbed system that can be simulated using numerical methods; characteristic relaxation time is compared to the numerically found results in section 4.1.

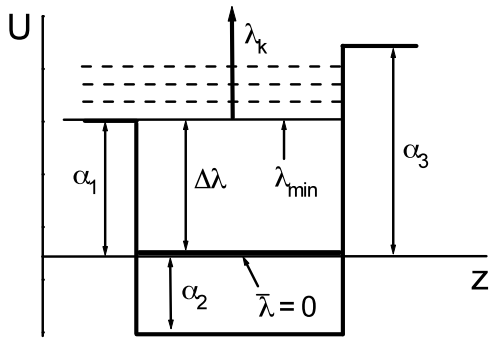

Figure 17. The associated potential of the linearized problem being related to the pseudolinear model of the bistable system.

3.2.2 Adiabatic approximation

The adiabatic approximation is a useful tool to understand the mechanism of the quasi-stationary (quasi-statically slowly) driven BFs that ignores time delays between the ac force $f(t)$ and the speed function $c(t)$ of the ac driven BF. Also it can be used to investigate the spurious drift of BFs under strong ac forcing. The adiabatic approximation fits well in the case of slowly oscillating forcing when u_t is removed from the governing equation (58):

$$\begin{aligned} &u_{zz} + c_M s_A(t)\, u_z - R_F(u) = 0, \\ &R_F(u) = R(u) - f(t), \end{aligned} \tag{81}$$

where the notation $s_A(t)$ stands for the "instantaneous" speed function i.e., it describes the immediate, instantaneous response of BF to the applied force. The governing equation of the quasi-stationary driven BF (81) bears a close similarity to that of the free, unperturbed BF; both the speed functions and the front solutions of the slowly driven BFs derivable by the piecewise linear rate function (48) are known explicitly [5, 15]. The scaled speed functions $s(t)$ are the main subject of the present research. The "instantaneous" speed functions $s_A(t)$ that ignore the time lags discussed are derivable by use of the "speed equation" being derived by the direct solution of (81). The speed equation reads (see [5, 15] for details)

$$\frac{\Psi_{Sn}[s_A(t)]}{\exp(-\varphi[s_A(t)])\ \sin\Phi(s_A(t))} = \frac{h_R - (1+h_R)f(t)}{1+(1+h_R)f(t)}, \tag{82}$$

where the auxiliary functions are defined by the relations

$$\begin{aligned} &\varphi(s_A) = \frac{s_A\Phi(s_A)}{Q_2(s_A)}, \qquad \Psi_{Sn}(s_A) = F_{Sn}/F_V, \\ &\Phi(s_A) = \begin{cases} \arctan\Psi_{Tg}(s_A), & \Psi_{Tg}(s_A) > 0, \\ \pi - \arctan(-\Psi_{Tg}(s_A)), & \Psi_{Tg}(s_A) < 0, \end{cases} \end{aligned} \tag{83}$$

and the unknown functions are described as follows:

$$\begin{aligned} F_{Sn} &= Q_2(s_A)[\delta_1 K_1(s_A) - \delta_3 K_3(s_A)], \\ F_V &= Q_2^2(s_A) + G_1^2(s_A), \\ \Psi_{Tg}(s_A) &= F_{Sn}/F_{Cn}, \\ F_{Cn} &= -[Q_2^2(s_A) + G_1(s_A)G_3(s_A)], \end{aligned} \tag{84}$$

where

$$\begin{aligned} &Q_2(s_A) = \sqrt{1-s_A^2}, \\ &K_{1,3}(s_A) = -s_A \pm \sqrt{r_{1,3}+s_A^2}, , \\ &G_{1,3} = -s_A + \delta_{1,3}K_{1,3}(s_A). \end{aligned} \tag{85}$$

The characteristic parameters $\delta_{1,3}$ and $r_{1,3}$ are described by the relations: $\delta_{1,3} = \alpha_2/\alpha_{1,3}$ and $r_{1,3} = \delta_{1,3}^{-1}$. The boundary conditions $u(z \to \mp\infty) \to u_{1,3}$ have been used in the derivation of these equations.

In general, the ac driven BF follows behind the time-dependent forcing with some lag (retardation); the actual speed functions $c(t)$ are retarded with respect to the applied forcing $f(t)$. The adiabatic approximation of the equation (58) ignores the time lags (retardation effects) between the ac force $f(t)$ and the speed function $c(t)$ of the ac driven BF. The quasi-stationary ac drive is of the highest "efficiency" in terms of the speed rectification discussed; it always induces the maximal shift of the mean drift velocity $< c(t) >$ of the ac driven front, as shown in [17].

3.3 Computer modeling

Mathematical model for finding both, the front-solutions and the propagation rates of ac driven BF, and numerical algorithm to solve it are described in this section. As it has been indicated before, the rigorous analytical methods for solution of the governing equation (58) are lacking; there is no general method of finding analytical solutions of the nonlinear partial differential equation (58). The perturbation theory describes only the weakly perturbed systems and is of limited use. Seeking to find both the front-solution $u(z,\ t)$ and the speed function $s(t)$ of the ac-driven BF, the numerical method of the finite differences [65] was employed. The method approximates derivatives by finite differences and has been chosen over other methods such as Finite element methods or spectral methods due its simplicity. The equation (58) can be solved using mathematical application packages like Maple, Matlab, or Mathematica [66-68] but due to traveling solution and specific forcing functions it is not convenient to work with them. Consequently, algorithm has been created and then implemented using Java programming language [69-71].

3.3.1 Mathematical model

To numerically find both the perturbed front-solutions $u(z,\ t)$ and velocity function $c(t)$ one needs initial and boundary conditions of the governing equation (58). Therefore, mathematical model has two parts: (a) homogeneous problem when the free, unperturbed front-solution $u_0(z,\ t)$ is found and (b) non-homogeneous problem when the velocity $c(t)$ of the propagating front $u(z,\ t)$ is obtained. Namely, two steps are needed to calculate the solution of the non-linear parabolic type PDE (58). In the first step homogeneous problem (5) with the piecewise-linear rate function $R(u)$ (48) is solved, when no external forces ($f(t) = 0$) applied on the front. Therefore, the Cauchy problem is formulated for the non-linear parabolic type PDE (5) in one-dimensional case with the initial conditions

$$u(z,\ t=0) = a\ \tanh(qz) + b,\ -\infty < z < +\infty, \tag{86}$$

where a, q and b denote the parameters described by the relations

$$a = q = \frac{(u_3 - u_1)}{2} \text{ and } b = \frac{(u_3 + u_1)}{2}. \tag{87}$$

The approximate function (86) is used to find initial condition of the governing equation (58). The boundary conditions of the equation (5) can be obtained from the algebraic equation:

$$\{u_t\} + R(u) = 0 \rightarrow R(u) = 0. \tag{88}$$

One can see that the equation (88) has three solutions $u = u_1,\ u_2,\ u_3$, but as it was shown in phase portrait, the free BF solution $u_0(z,\ t)$ joins the outer zero-points of the rate function, u_1 and u_3, that describe the stable states of the system. The boundary conditions of the homogeneous problem are

$$u(t;\ z \rightarrow -\infty) = u_1 \text{ and } u(t;\ z \rightarrow +\infty) = u_3,\ t > 0. \tag{89}$$

After solving the presented Cauchy problem using a numerical method the free, unperturbed BF solution $u_0(z,\ t)$ propagating at some fixed velocity c_0 is found.

In the second step non-homogeneous problem (58) with the piecewise-linear rate function $R(u)$ (48) is solved. The stationary-steady solution $u_0(z,\ t)$ to homogeneous problem is used as the initial conditions of the non-homogenous problem. Boundary conditions of governing equation (58) are obtained from the solution of the following equation:

$$u_t + R(u) = f(t). \tag{90}$$

This equation follows from the governing equation (58) by taking into account that $z \rightarrow \pm\infty$, then $u_z \rightarrow 0$ and $u_{zz} \rightarrow 0$. The initial conditions of the problem (90) are $V_1(t = t_0) = u_1$ and $V_3(t = t_0) = u_3$, where u_1 and u_3 are the boundary conditions of the homogeneous ($f(t) = 0$) problem. The formulated Cauchy problem is used to find both the front-solution $u(z,\ t)$ and the speed function $s(t)$ of the ac driven BF numerically.

3.3.2 Finite difference method

Finite difference method is used to find the front-solution. The first step is to discretize the problem's domain by dividing it into a uniform grid. In case of the function $u(x,t)$ of two arguments we should work on the rectangular domain $\overline{D} = \{0 \le x \le X, 0 \le t \le T\}$. The segment $[0,X]$ on the x-axis is divided into N equally spaced grid steps $h = X/N$ at points $x_i = ih$ indexed by $i = 0,1,...,N$, and the segment $[0,T]$ is divided into M steps $k = T/M$ at points $t_j = jk$, $j = 0,1,...,M$. This way we get the nodes (x_i,t_j), which constitute a widespread grid [65]:

$$\overline{\omega}_{hk} = \{(x_i,t_j) \in \overline{D}\}. \tag{91}$$

The space of solutions to the differential equation (58) is approximated by the space of grid functions:

$$u_i^j = u(x_i,t_j) \tag{92}$$

The second step is to approximate derivative expressions in PDEs by finite differences. A *forward difference* for the t-derivatives and a second-order *central difference* for the second x-derivative of $u(x,t)$ with the local truncation error of order $O(k)$ and $O(h^2)$, respectively, are derived from Taylor series expansions:

$$\frac{\partial u}{\partial t} = \frac{u_i^{j+1} - u_i^j}{k} \text{ and } \frac{\partial^2 u}{\partial x^2} = \frac{u_{i+1}^j - 2u_i^j + u_{i-1}^j}{h^2}. \tag{93}$$

The third step - solving the difference equations subject to the prescribed boundary and initial conditions. The following expression is obtained by substituting approximations (93) into the equation (58) without moving coordinates:

$$\frac{u_i^{j+1} - u_i^j}{k} - \frac{u_{i+1}^j - 2u_i^j + u_{i-1}^j}{h^2} + R(u_i^j) = f(t_j). \tag{94}$$

Solving this equation for u_i^{j+1} gives the explicit solution

$$u_i^{j+1} = (1-2r)u_i^j + r(u_{i+1}^j + u_{i-1}^j) + k(f(t_j) - R(u_i^j)) \tag{95}$$

where $r = k/h^2$. The result of this is called an *explicit finite-difference* scheme. Values at time t_{j+1} can be obtained from the corresponding values at time t_j.

Using this recurrence relation, numerical approximations of $u(x_i,t_j)$ are only computed at internal nodes of the grid $\overline{\omega}_{hk}$:

$$\omega_{hk} = \{(x_i,t_j) \in \overline{D}\}\ ,\ i = 1,...,N-1,\ j = 1,...,M \tag{96}$$

where the set of all boundary nodes is denoted as $\gamma_{hk} = \overline{\omega}_{hk} - \omega_{hk}$. Now, we need to know the values of u_0^j and u_N^j on the boundaries. The boundary conditions (89) of the initial problem can be approximated as follows:

$$u_0^j = u_1 \text{ and } u_N^j = u_3. \tag{97}$$

Approximation of the initial conditions (86):

$$u_i^0 = a\ \tanh(q\ x_i) + b,\ i = 1,...,N-1. \tag{98}$$

where the parameters a, q and b are defined in (87). The boundary conditions (90) of the non-homogeneous problem is found from the following approximation:

$$u_i^{j+1} = u_i^j + k(f(t_j) - R(u_i^j)) \tag{99}$$

with the initial conditions for the left boundary, $u_0^0 = u_1$, and the right boundary, $u_N^0 = u_3$. The initial conditions of the non-homogenous problem are obtained from the stationary-steady solution $u_0(z,\ t)$.

This explicit schema is numerically stable and convergent if the following condition is applied [65, 72]:

$$r \le 1/2\,. \tag{100}$$

In addition, the local truncation error is

$$T_h = O(k + h^2)\,. \tag{101}$$

In order to decrease the truncation error by using a finer grid may result the increase of *round-off error* due to increased number of arithmetic operations. Taking that into account, the time step $k = 0.001$ and the space step $h = 0.05$ were chosen to use for all numerical calculations to achieve accurate results.

The *explicit* method was chosen for all calculations due its simplicity, high calculation speed (number of arithmetical operations is proportional to $(N+1) \times M$) and adequate results. The *implicit* and *Crank-Nicholson* methods were considered due their stability, time step but for the given problem explicit method was sufficient.

3.3.3 Velocity of Bistable Front

To find the speed function $c(t)$ of the ac driven BF, the equation (58) was approximated by the finite difference scheme in the co-moving coordinates, $z = x - x_C(t)$, with the traveling center of the ac driven front, $x_C(t)$. The actual speed functions $c(t)$ that follow behind the ac force with some retardation have been obtained by considering the traveling center $x_C(t)$ of the BF:

$$c(t_t) = \frac{x_C(t_j) - x_C(t_{j-1})}{t_j - t_{j-1}} = \frac{\Delta x_c}{\Delta t}, \tag{102}$$

where variable Δx_C denotes the displacement of the traveling center $x_C(t)$ of the BF. The position of the traveling center of the running front in the rest frame is given by the expression

$$x_C(t) = \frac{\int_{-L}^{L} dx\ x\ u_x(x,t)}{\int_{-L}^{L} dx\ u_x(x,t)}. \tag{103}$$

Here $-L$ and L stand for the left and right edges of the regional domain $\overline{D}$, respectively. As it was mentioned, the scaled speed function $s(t) = c(t)/c_M$, $c_M = 2\sqrt{\alpha_2}$, is used to present results.

3.3.4 Algorithm

Computer algorithm for finding both the front-solution $u(z,\ t)$ and the speed function $s(t)$ of the ac-driven BF consists of two parts: firstly, solving homogeneous problem (5), (86), (89) and, secondly, non-homogenous problem (58), (90). Algorithm for the homogeneous problem consists of the following steps:

- First of all, initial parameters of the rate function ($\alpha_{1,2,3}$, g_H, ΔR, u_2) and grid (k and h - grid steps, N- number of steps along the x-axis) are set. In addition, parameters for the particular force function are provided.
- Boundary conditions, u_1 and u_3, are calculated using initial parameters.
- Initial conditions at $t = 0$ are calculated using (86).
- For each time-step, the problem (94) with $f(t) = 0$ is solved and the

speed value is calculated using (102). Moreover, in order to achieve that coordinate system is moving together with the front solution, the displacement variable x_{disp} is calculated by adding value of displacement of weight center Δx_C. For each iteration the following conditions are checked:

- If $x_{disp} < h$, then coordinate system is not shifted.
- If $x_{disp} \geq h$, then coordinate system is shifted and value of x_{disp} has to be adjusted as follows: $x_{disp} = x_{disp} - \lfloor x_{disp} / h \rfloor * h$.

During numerical procedure the speed s_0 and its deviation Δs_0 are calculated. Finally, stationary solution $u_0(z, t)$ is obtained and numerical procedure can be stopped, when condition, $\Delta s_0 \leq 0.01$, is satisfied. It means the speed of the BF is been calculated by 1% accuracy ($s \cong const$) and the shape of the front solution is stable. After solving the homogeneous problem the free, unperturbed BF solution $u_0(z, t)$ propagating at some fixed velocity s_0 is found.

Similarly, algorithm solving the non-homogeneous problem is described as follows:

- A particular oscillating force function $f(t)$ is calculated. In addition, the zero-time average condition, $< f(t) >= 0$, is satisfied.
- Boundary conditions are obtained using the equation (90).
- The stationary-steady solution $u_0(z, t)$ is applied as initial conditions.
- For each time-step, the problem (94) with $f(t) \neq 0$ is solved and the speed value is calculated using (102). Moreover, the coordinate system is moving together with the front solution in the same manner as before.

Numerical procedure cannot be stopped the same way as in homogeneous case because force acting on the front is quasi-periodic or quasi-noisy and speed of BF is changing accordingly. In this case the zero-time average condition, $< f(t) >= 0$, is a good stopping criterion. In addition to that, one has to assure minimum number of periods, i.e. $T > 10$, when slow (quasi-

stationary) forcing is applied. As a result, both the front-solution $u(z, t)$ and the speed function $s(t)$ of the ac-driven BF are found.

3.3.5 Implementation

The algorithm described has been implemented using Java programming language because of the moving coordinate system and ability to have full control of the process. Implementation has been done using two different arrays: one containing front-solution $u(z)$ at time-step t and another at time-step $t-1$. Arrays are exchanged at the next time-step when a new front solution is calculated using the equation (95). This way the exploitation of the memory is very effective. In addition, the boundary conditions has been calculated and stored in separate arrays. In order to save calculation time and to use the same random generated values of the qausi-noisy force, text files have been used.

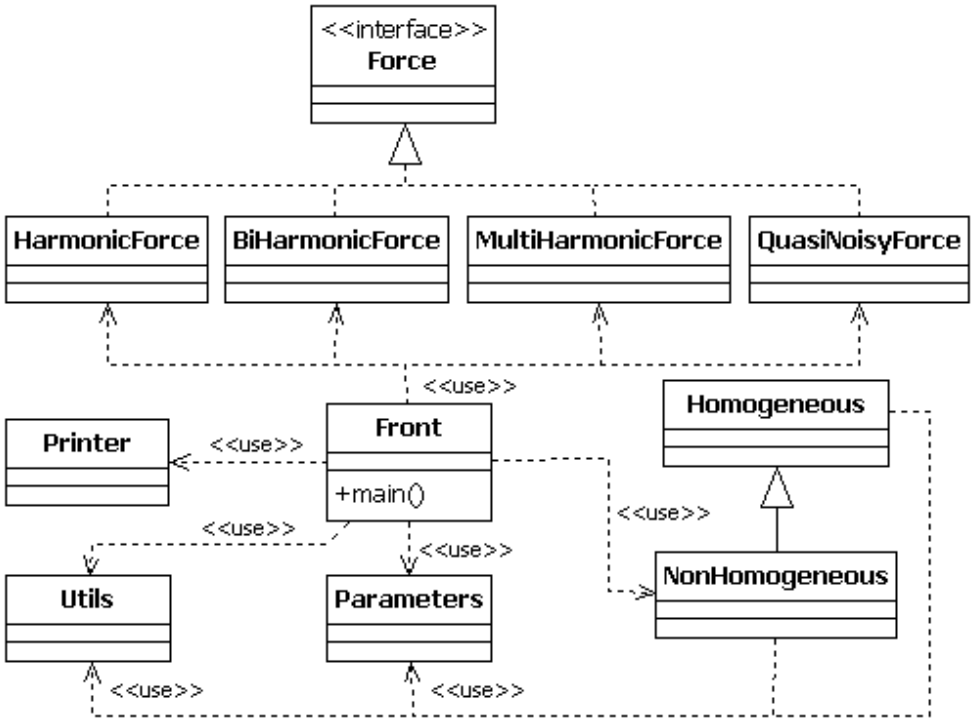

Figure 18. Class diagram

Regarding software architecture Apache Ant tool has been used to compile, build and run the program using command-line interface without additional parameters. Its advantage - a convenient way to schedule needed calculations

using time-based job schedulers like Cron because depending on the hardware calculations may take a long time. All the initial parameters have been stored in a properties file that is convenient to read when object of all parameters are created. The homogeneous and non-homogeneous problems were separated into two different classes as it is shown in class diagram in Figure 18. In addition, all force functions have been implemented in separate classes having the same interface. Printer class has been created to print results into a file and to display intermediate results using jFreeChart charting library. Besides, final results have been exported into CSV file format and visualized using Origin application software. Finally, Apache log4j framework has been used for logging.

4. Results

The results obtained using both the numerical simulations and analytic tools are presented in this chapter. The principal objective is to investigate new possibilities of controlling the directed net motion of the self-ordered BF by the periodic and stochastic zero-mean ac forces. The average characteristics of the ratchet-like transport, that describe the dependence of the average drift velocity of the ac-driven front versus both the amplitude f_0 and frequency ω_0 of the driving force, are studied in a wide interval of both the parameters f_0 and ω_0, for the arbitrary strengths and the "rates" of the driving forces used. To better illustrate ratchet effect the acceleration factor ρ that characterizes the magnitude of the average acceleration of the ac-driven front is calculated

This chapter has four sections presenting results derived using different forcing function. First, control possibilities of the BF with a retarded response to the single-harmonic forcing are investigated using asymmetrical rate functions. Section 4.2 deals with the "efficiency" of the ratchet-like shuttling of the quasi-periodically forced BFs. Then the "efficiency" of the multi-harmonic force is examined in section 4.3. Finally, the noise-induced drift of BFs under the bounded noise forces with different spectral content is investigated in the last section.

4.1 Periodically forced fronts: single-harmonic forcing

The occurrence of the time lags (retardation effects) τ_D between the oscillatory force and the instantaneous velocity of the periodically forced BFs being described by the *symmetrical* rate functions has influence on the spurious drift of BFs, as was shown in [57, 59]. In this section the influence of the retardation effects on the ratchet-like transport of the ac driven fronts being described by the *asymmetrical* rate functions (48) are investigated.

In considering the ratchet-like shuttling of BFs, the oscillatory force $f(t)$ acting on the front in the system is approximated by the single-harmonic forcing function of the highest temporal symmetry (59). Such forcing function

was chosen to demonstrate better the influence of $R-u$ symmetry on the ratchet-like transport. In addition to the scaled speed function $s(t)$, the scaled forcing functions $f^*(t)$ being defined by the relation $f^*(t) := f(t)/\Delta R$ are preferable, in considering the ratchet-like transport of the BF. The average characteristics of the spurious drift of BFs derivable by the self-similar rate functions $R(u; C)$ (45) are not sensitive to the height ΔR of the rate function (48) if both scaled functions $f^*(t)$ and $s(t)$ are used [15, 17, 57].

Before discussing retardation effects, ratchet-like transport of BFs ignoring time lags is illustrated in Figure 19, where the "instantaneous" oscillatory function $s_A(t)$, followed from the speed equation (82), is presented for the single harmonic forcing $f^*(t)$ described by the relation (59). Before the oscillatory forcing is switched on, the free, unperturbed BF travels at steady speed s_0. Then the oscillations of the velocity of BF instantaneously start to follow applied slow forcing.

In general, the retardation effects always take place when the periodic oscillatory zero-mean ac forces being capable to induce the directed net motion are applied on the BFs. In case of the fast driving (fast changing oscillations), the front dynamics with a delayed, postponed reaction of BF to the oscillatory force $f(t)$ (59) is studied numerically, by the direct solution of the governing equation (58). The oscillatory speed functions $s(t)$ that are derived numerically at the different slope coefficients α_3 are presented by the solid curves in Figure 20. On the other hand, the slow ac drive that describes almost immediate, nearly "instantaneous" response of BF to the applied forcing is studied analytically using the adiabatic approximation (81). Accordingly, the dashed curves in Figure 20 show the instantaneous speed functions $s_A(t)$ being derived using adiabatic approximation. The actual speed functions $s(t)$ become more and more flattened with the decreasing slope coefficient α_3 (compare the solid curves shown in the figure). In other words, the magnitude, $\Delta s = s_M - s_m$, of the oscillatory function $s(t)$ and the lag time between both $s-t$ and s_A-t dependences increase with the decreasing slope coefficient α_3, in accord with

relation (80); the subscripts M and m denote "Maximal" and "minimal", respectively. The increasing time lags τ_D between both oscillatory functions $s(t)$ and $s_A(t)$ are schematically depicted by the straight inclined lines (a) and (b) denoting the average "slopes" of the considered $s_A - t$ and $s - t$ dependences (the straight inclined line indicating the average "slope" of the oscillatory function joins the adjacent extremes of the oscillatory function). One can see that the relative slope between both inclined lines (a) and (b) increases with the decreasing slope coefficient α_3 (compare the separate families of the curves labeled (A), (B) and (C) in the figure). Notice that the magnitude of the actual (retarded) speed function, Δs, becomes notably reduced even at the moderately low frequencies satisfying the relation $\omega \cong \tau_R^{-1}$. Also, the amplitude of the functions $s(t)$ is proportional to $\tan\beta$, where β is an angle between line (b) and horizontal axis.

Referring to the particular case labeled by (B) in the Figure 20, the relation $\Delta s / \Delta s_A \approx 0.3$ holds, where the quantity, $\Delta s_A = s_{AM} - s_{Am}$, denotes the magnitude of the "instantaneous" oscillatory function $s_A(t)$ (82) that ignores time lags. Even in case of "normal" driving, $\omega\tau_R = 1$, the influence of retardation effects on the spurious drift of the BF is very distinct. It is necessary to note that both parameters τ_R^{-1} and ω that characterize the "rate" of the system and the oscillatory force, respectively, are of the same order in magnitude in this case, namely, one has that $\omega = 6\tau_R^{-1}$ (see the figure caption). The oscillatory speed functions $s(t)$ become very flattened, namely, the inequality $\Delta s << \Delta s_A$ holds if the criterion of the rapid driving, $\omega\tau_R >> 1$, is satisfied, as follows from direct calculations.

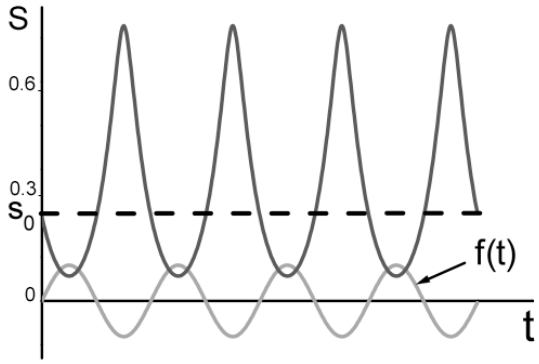

Figure 19. Illustration of the ratchet effect. The "instantaneous" velocity of the bistable front driven by the single harmonic forcing $f^*(t) = f_0^* \sin \omega t$. The initial velocity s_0 of BF is shown by the dashed line. The parameter values are $f_{Mx} = -R_m$, $r_1 = 10$, $r_3 = 0.1$ and $h_R = 9.5$.

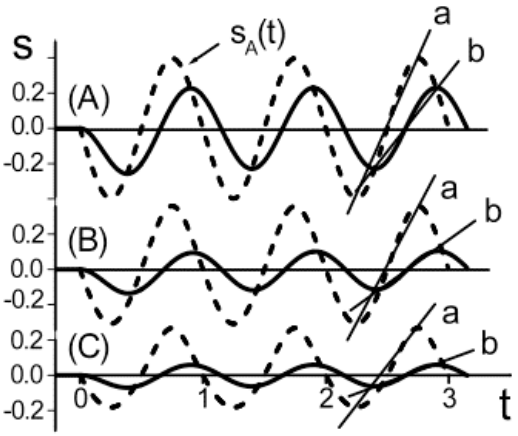

Figure 20. The retarded speed functions $s(t)$ being derived at the different values of the outer slope coefficient α_3 (shown by the solid curves). The dashed curves show the "instantaneous" speed functions $s_A(t)$ that ignore delays. The average slopes of both speed functions $s_A(t)$ and $s(t)$ are depicted by the straight inclined lines (a) and (b), respectively. The relative slope (angle) between both lines (a) and (b) increases with the increasing slope coefficient α_3. The parameter values are: $f_0^* = 0.6 f_{Mx}^*$, $T = 1$; $\alpha_1 = 5$, $\alpha_2 = 1$, $h_R = h_0$, $s_0 = 0$; (curves A) $\alpha_3 = 5$, $T = 5\tau_R$, $h_R = 1$; (curves B) $\alpha_3 = 1$, $T = \tau_R$, $h_R = 1.29$; (curves C) $\alpha_3 = 0.2$, $T = 0.2\tau_R$, $h_R = 2.24$. The forcing amplitudes f_0^*, being related to the separate pairs of the curves labeled by *A*, *B*, and *C* are as follows: $f_0^* \approx 0.30$, 0.26, and 0.19, respectively.

The influence of the retardation effects discussed on the ratchet-like transport of BFs is demonstrated by $v - \omega$ dependences shown by the solid curves 1, 2, and 3 in Figure 21. Here v stands for the mean drift velocity of the ac driven BF and was calculated numerically. Notice that the average characteristics shown by curves 1 and 2 are derived with the asymmetrical rate function while the particular case of the symmetrical rate function is presented by curve 3. The relaxation rates τ_R^{-1} being related to the separate curves 1, 2, and 3 are as follows: τ_R^{-1}=0.2, 1.0, and 5.0, respectively. One can see that the presented $v - \omega$ dependences with the lesser values α_3, namely, $\alpha_3 = 0.2$ and $\alpha_3 = 1.0$, that are related to the lower characteristic rates τ_R^{-1} and the larger lags τ_D are more steeply sloped, in accord with relation (80).

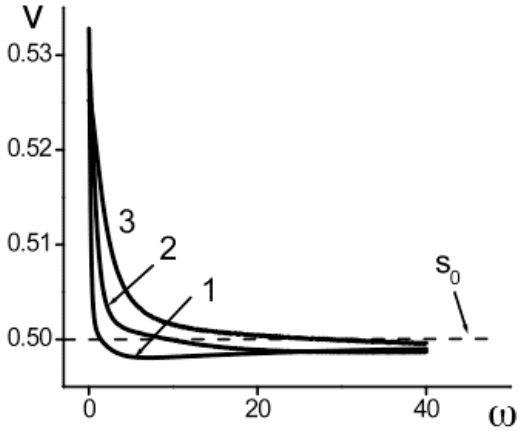

Figure 21. The mean drift velocity of the ac driven BF versus the frequency of the harmonic force. The initial velocity of BF (shown by the dashed line) was taken fixed, namely, $s_0 = 0.5$. The parameter values are: $f_0^* = 0.9 f_{Mx}^*$; $\alpha_1 = 5$, $\alpha_2 = 1$, $h_R = h_0$; (curve 1) $\alpha_3 = 0.2$, $h_R \approx 9.6 h_0$ ($h_0 \approx 2.24$), $f_0^* \approx 0.04$; (curve 2) $\alpha_3 = 1.0$, $h_R \approx 6.9 h_0$ ($h_0 \approx 1.29$), $f_0^* \approx 0.09$; (curve 3) $\alpha_3 = 5.0$, $h_R \approx 6.3 h_0$ ($h_0 \approx 1.00$), $f_0^* \approx 0.12$. The characteristic time durations τ_R being related to the separate curves (1), (2), and (3) are as follows: τ_R=5.0, 1.0, and 0.2, respectively. Notice that the steepness of the given $v - \omega$ dependences increases with the decreasing slope coefficient α_3. In the range of the high frequencies satisfying the relation $\omega\tau_R >> 1$ the mean drift velocity of BF is very close to that of the free BF, s_0, i.e., the spurious drift of BF practically disappears.

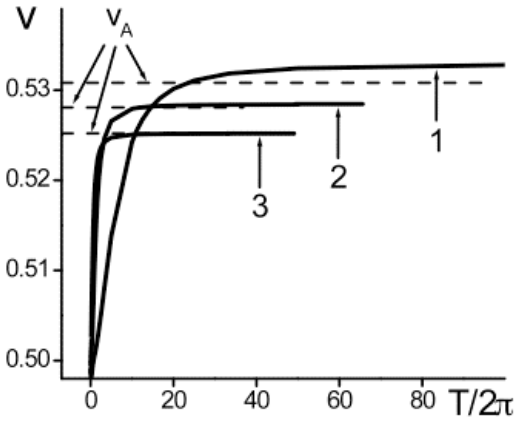

Figure 22. The same as in Figure 21, but the dependence of the mean drift velocity of BF versus the period of the ac force is presented. Both the denotations and the parameter values are the same as in Figure 21. The dashed horizontal lines show the mean drift velocities v_A being derived by the speed equation (82); these are as follows: (curve 1) $v_A \approx 0.531$; (curve 2) $v_A \approx 0.528$; (curve 3) $v_A \approx 0.524$. The actual drift velocities v, when taken at the fixed period, $T = 100$, which satisfies the relation $T >> \tau_R$, are as follows: (curve 1) $v \approx 0.533$; (curve 2) $v \approx 0.528$; (curve 3) $v \approx 0.525$.

Worth to mention that the "acceleration factor" of the ac driven BF, $\rho := |s_0|^{-1} v$, which characterizes the "efficiency" of the ac driver, becomes notably reduced, i.e., the drift velocity v of the ac driven BF becomes very close to that of free, unperturbed BF, s_0, even at "moderately low" frequencies ω satisfying the relation $\omega\tau_R \cong 1$. More specifically, the acceleration factors, $\rho_R \equiv \rho(\omega = \tau_R^{-1})$, being related to the separate R curves 1, 2, and 3 shown in Figure 21 are as follows: 1.03, 1.02, and 1.01, respectively.

The dependences of the mean drift velocity v versus the period T of the forcing are used to analyze the peculiarities of the ratchet-like shuttling of BFs in the low-frequency range of the oscillatory force and are presented in Figure 22; both the notations and the parameters used are the same as in Figure 21. As

expected, the average $v-T$ characteristics are decreasingly sloped with the increasing period of the forcing function. The mean drift velocity v of the ac driven BF becomes very close to that of the quasi-stationary driven BF, v_A, if the period T of the ac force significantly exceeds the characteristic relaxation time of the system, τ_R. As a result, the lag time τ_D between the ac force $f^*(t)$ and the speed function $s(t)$ of the ac driven BF practically vanishes if the criterion of the slow driving $T >> \tau_R$ is satisfied. In other words, the retardation effects become notably reduced and this result well corresponds to the previous findings (see Figure 20).

Regarding the peculiarities of the reversal behavior of the directed net motion of the ac driven BFs derivable by the asymmetrical rate functions are investigated in the rest of this section. The BF driven by the time-symmetric oscillatory force of zero-time average exhibits the reversal of the unidirectional net motion by changing value of the amplitude of the ac force. The reversal implies that the average $v-f_0^*$ characteristic of the ac driven BF has at least one null (zero-point). The rigorous criteria under which the reversals discussed exist (occur, vanish) are lacking because the governing equation (58) is analytically not solvable. The approximate criteria being derived using adiabatic approximation, more exactly, the necessary, but insufficient conditions for the existence of the reversals discussed are obtainable by considering the spurious drift of BFs under "slow" ac forcing satisfying the relation $T \to \infty$ [15]. The approximate criteria encompassing both cases of the backward- and forward-running BFs satisfying the relations $s_0 < 0$ and $s_0 > 0$, respectively, read: (A) $h_R \in (1, h_0)$ if $\alpha_1 > \alpha_3$ (the particular case, $s_0 < 0$); (B) $h_R \in (h_0, 1)$ if $\alpha_1 < \alpha_3$ (the other case, $s_0 > 0$); the boundary conditions $u_0(z \to \mp\infty) \to u_{1,3}$ have been used in the derivation of these relations. The adiabatic approximation being used in the derivation of the presented relations (A) and (B) ignores the time lags between the instantaneous velocity of the ac driven BF and the ac forcing. Accordingly, numerical simulations have been used because it is not clear enough whether and how strongly the retardation

effects discussed are capable to influence on the reversal behavior of the unidirectional net motion of the ac driven BFs.

The numerically found $v - f_0^*$ dependences encompassing both cases of the progressive and regressive (decelerated and accelerated) dc motion of BFs are presented by the solid curves in Figure 23 and Figure 24, respectively. One can see that the numerically found $v - f_0^*$ dependences that describe the particular case of the slow oscillatory force satisfying the relation $T >> \tau_R$ agree well with the appropriate $v_A - f_0^*$ dependences being derived within the adiabatic approximation by the speed equation (82) (compare the solid and the dashed curves labeled by a and v_A, respectively, in both figures). The steepness of the given $v - f_0^*$ characteristics decreases with the frequency of the ac force being increased. In other words, the spurious drift of BF becomes notably suppressed in the whole interval of the driving amplitudes f_0 if the period of the ac force becomes lesser if compared to the characteristic relaxation time of the system, namely, if the relation $T \le \tau_R$ is satisfied (see curves labeled by c in Figure 23 and Figure 24). In addition, the particular case of the "regressive-progressive" dc motion exhibiting the reversal that satisfies the criterion (A) is demonstrated by curve (a) in Figure 24.

The occurrence of the time lags in the oscillatory motion of BF leads to the shifting of the nulls of $v - f_0^*$ characteristic toward the larger values of the driving amplitude f_0^*. Referring to the "critical" case labeled by b in the Figure 24, the ac driven front, which initially propagated at some fixed nonzero velocity s_0, experienced the stopping (directed net motion of the self-ordered front is stopped) at the maximal amplitude, $f_0^* = f_{Mx}^*$, above which the global stability of BF breaks down. The higher oscillatory frequency ω leads to the larger lags and results the average $v - f_0^*$ characteristic becomes more flattened. As a consequence, the "reversal" of the unidirectional net motion of the BF disappears (see curve c in Figure 24). In addition, the average $v - f_0^*$ characteristics become very flattened practically in the whole interval of the driving amplitudes f_0^* if the lag time τ_D significantly exceeds the period of the

forcing, namely, when the criterion of the fast driving $\omega\tau_R >> 1$ is satisfied, as follows from the numerical simulations. As noted, the rigorous criteria for the occurrence of the reversals discussed are lacking. The reversals will disappear almost in the whole interval of the initial propagation rates s_0 of the ac driven BF if the criterion of the rapid driving is satisfied, as follows from the direct calculations.

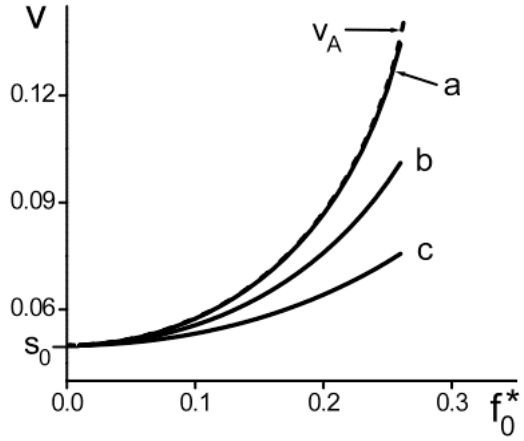

Figure 23. The mean drift velocity of the ac driven BF versus the amplitude of the harmonic force. The solid curves (a), (b), and (c) show the actual $v - f_0$ dependences being derived by the numerical solution of equation (58); the dashed curve labeled by v_A is obtained by the speed equation (82). The parameter values are: $\alpha_1 = 5$, $\alpha_2 = 1$, $\alpha_3 = 0.2$, $h_0 \approx 2.24$, $h_R \approx 2.78$, $s_0 = 0.05$, $\tau_R = 5.0$; (curve a) $T/\tau_R = 60$; (curve b) $T/\tau_R = 10$; (curve c) $T/\tau_R = 5$. The maximal drift velocities v_{Mx} being derived at the maximal amplitude of the ac drive, $f_0^* = f_{Mx}^*$, are as follows: (curve a) $v_{Mx} \approx 0.13$; (curve b) $v_{Mx} \approx 0.10$; (curve c) $v_{Mx} \approx 0.08$.

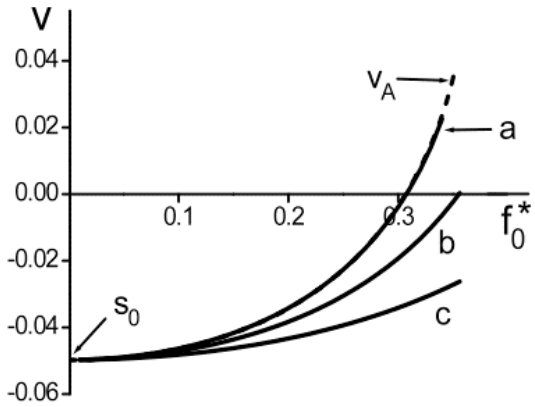

Figure 24. The same $v - f_0$ dependences as in Figure 23, but for the case of the oppositely running BF satisfying the criterion of the reversal behavior. The parameter values are: $\alpha_1 = 5$, $\alpha_2 = 1$, $\alpha_3 = 0.2$, $h_0 \approx 2.24$, $h_R \approx 1.81$, $s_0 = -0.05$, $\tau_R = 5.0$; (curve a) $T/\tau_R = 60$; (curve b) $T/\tau_R = 10$; (curve c) $T/\tau_R = 5$. The maximal drift velocities v_{Mx} being related to the separate curves a, b, and c are as follows: (curve a) $v_{Mx} \approx 0.042$; (curve b) $v_{Mx} \approx 0.000$; (curve c) $v_{Mx} \approx -0.026$. Notice that depending on the frequency of the driving force, the bistable front, which initially propagated at the fixed velocity s_0, exhibited (i) the reversal (curve a), (ii) the stopping (curve b), (iii) regressive (decelerated) dc drift (curve c), as a function of the driving amplitude.

4.1.1 Summary

The influence of the retardation effects (time lags) on the ratchet-like shuttling of BFs derivable by the asymmetrical rate functions was investigated in this section. By numerically simulating the drift motion of the ac driven BF under the single-harmonic ac forcing the following conclusions were made:

- The lag time τ_D between the instantaneous velocity of the ac driven BF and the oscillatory forcing is a function of the outer slope coefficients of the rate function and is not sensitive to the inner; furthermore, it has only weak dependence on the strength of the applied forcing.
- The retardation effects (time lags) in the front dynamics are describable adequately enough by use of the perturbation theory.
- The occurrence of the time lags in the oscillatory motion of the ac driven BF being described by the asymmetrical rate functions shrunk the spurious drift of BF; the spurious drift of BFs practically disappeared if the frequency of the oscillatory force acting of the front significantly exceeded the characteristic relaxation rate of the system.
- The possibilities of controlling the directed net motion of the self-ordered fronts by the low- and high-frequency zero-mean ac forces radically differ: the occurrence of the time lags in the front dynamics leads to the vanishing of the reversals in the directed net motion of the ac driven BFs, being inherent in the case of the extremely slow (quasi-stationary) ac drive.

4.2 Quasi-periodically forced fronts: bi-harmonic forcing

The main aim of this section is to study the "efficiency" of the quasi-periodic, temporally irregular ac driver, in terms of the spurious drift of the driven BFs. Both cases of periodic $f_P(t)$ and quasi-periodic $f_Q(t)$ forcing functions being derived from the bi-harmonic forcing expression (60) are used to compare results. The "efficiency" of the oscillatory force of zero-time average may be evaluated by considering the acceleration factor, $\rho := |s_0|^{-1} v$, which denotes the relative increase of the mean drift velocity of the ac driven of BF. As previously noted, the spurious drift of BFs is very sensitive to the peculiarities of $f - t$ dependence; thus, it is not clear a priori, in advance whether and how strongly the temporally irregular ac forcing $f_Q(t)$ is capable to support the propagation of BF.

4.2.1 Self-ordered front under slow oscillatory force

The particular case of the slow oscillatory forces satisfying the relation $\mu\omega\tau_R << 1$ is used to study ratchet-like transport. As a result, the propagation velocity $s(t)$ of the ac driven BF almost instantly follows the ac force if the frequency of the fastest (super-harmonic) mode of the periodic bi-harmonic forcing function is much lesser than the characteristic relaxation rate of the system, τ_R^{-1} [57, 59]. Worth to notice that the periodic and extremely slow (quasi-stationary) ac force of zero-time average is of the highest "efficiency" in terms of the spurious drift discussed, namely, it always induces the maximal shift of the mean drift velocity of the ac driven BF [57]. Nevertheless, the temporal behavior of both forcing functions used, the periodic $f_P(t)$ and quasi-periodic $f_Q(t)$ one, radically differs. The average $\rho - f_a$ characteristics of the periodically and quasi-periodically forced BFs that are derived by use of both the symmetrical and asymmetrical rate functions are presented in Figure 25 and Figure 26, respectively. The curves labeled by P and Q refer to the periodically and quasi-periodically forced BFs, respectively. The solid curves show the actual, numerically found $\rho - f_a$ dependences being derived by the governing equation (58). The limiting case of the quasi-stationary driven BFs, namely, the average characteristics derivable by the speed equation (82) are shown by the dashed curves. From presented results in Figure 25 and Figure 26 follow that the performance of the ratchet-like shuttling of BFs is much lesser pronounced with the quasi-periodic, temporally irregular ac forcing. In particular, the average $\rho - f_a$ characteristics of the quasi-periodically driven BFs are more gently sloped if compared to those being derived by the rigorously periodic forcing $f_P(t)$, in the whole interval of the driving amplitudes f_a, in both cases the symmetrical and asymmetrical rate functions. More precisely, the maximal acceleration factors being related to the separate curves labeled by P and Q in Figure 25 are as follows, $\rho_P(f_{Mx}) \approx 2.5$ and $\rho_Q(f_{Mx}) \approx 1.7$ where the denotation, $\rho_{P,Q}(f_{Mx}) \equiv \rho_{P,Q}(f_a = f_{Mx})$, stands for the acceleration factor taken at the maximal amplitude of the ac forcing, $f_a = f_{Mx}$.

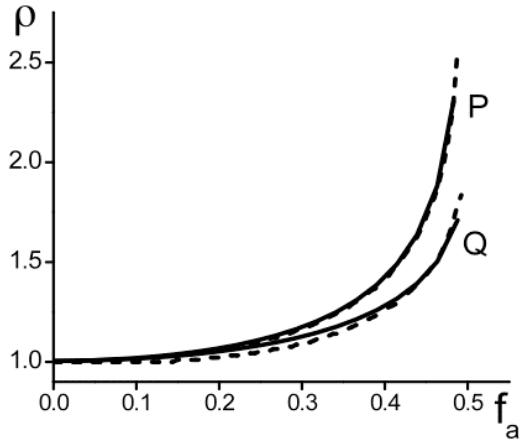

Figure 25. The acceleration factor ρ of the ac driven front versus the amplitude f_a of the ac force. The curves labeled by P and Q refer to the periodic and quasi-periodic forcing functions, respectively. The actual $\rho - f_a$ dependences that are derived by the governing equation (58) are shown by the solid curves; the period of the basic mode of both oscillatory forces was taken as follows, $T = 100\tau_R$. The dashed curves show the average $\rho - f_a$ characteristics being derived by the speed equation (82). The parameters of the symmetrical rate function used are as follows: $\alpha_1 = \alpha_3 = 1.0$, $\alpha_2 = 5.0$, and $h_R = 1.05$. The rest of the parameters are: $s_0 \approx 0.009$ and $\tau_R = 1.0$. The maximal acceleration factors $\rho_P(f_{Mx})$ and $\rho_Q(f_{Mx})$ being related to the separate curves P and Q are as follows: 2.5 and 1.7, respectively.

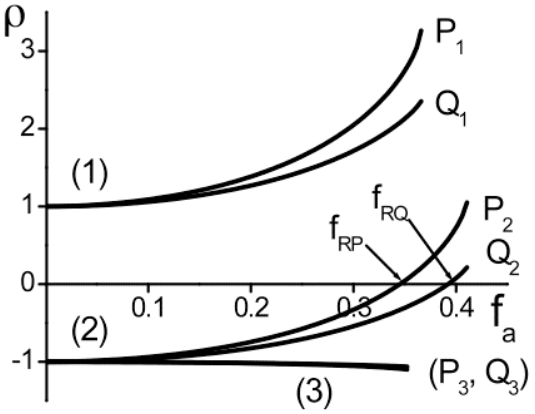

Figure 26. The same as in Figure 25 but for the other case of the asymmetrical rate function. The period of the basic mode of the oscillatory forces was taken as follows: $T = 100\tau_R$. The curves labeled by P_i and Q_i refer to the periodically and quasi-periodically forced BFs, respectively. The "critical" driving amplitudes $f_a = f_{RP}$ and $f_a = f_{RQ}$, at which the reversals of the directed net motion of the periodically and quasi-periodically driven BFs occur, are pointed by the arrows. Parameter values are as follows: $\alpha_1 = 5.0$, $\alpha_2 = 3.0$, $\alpha_3 = 1.0$, $h_0 \approx 1.58$ and $\tau_R = 1.0$; (curves (1)) $h_R \approx 1.74$, $s_0 \approx 0.024$; (curves (2)) $h_R \approx 1.44$, $s_0 \approx -0.024$; (curves (3)) $h_R \approx 0.55$, $s_0 \approx -0.261$.

Moreover, in case of the asymmetrical rate functions of the low R–u symmetry, the presented $\rho - f_a$ dependences in Figure 26 demonstrate different, dissimilar behavior for the periodically and quasi-periodically forced BFs. To be more specific, the average $\rho - f_a$ characteristics of the quasi-periodically driven BFs are more flattened than those derivable with the rigorously periodic forcing $f_P(t)$. As a result, the higher strength of the oscillatory force is required to achieve the reversal of the directed net motion of the ac driven BF, with the quasi-periodic, temporally irregular forcing $f_Q(t)$ in compare to the rigorously periodic forcing $f_P(t)$ (see curves P_2 and Q_2 in Figure 26). In addition, the "critical" amplitudes, $f_a = f_{RP}$, f_{RQ}, at which the reversals discussed take place are pointed by arrows in the figure. One can see

that both the periodically and quasi-periodically forced BFs will exhibit quite different, dissimilar behavior if the amplitude f_a of the oscillatory forces used is taken within the interval [f_{RP}, f_{RQ}]: the initial (free) BF, which propagates at the some fixed nonzero velocity s_0, will propagate, on average, in two opposite directions, depending on the particular ac forcing, either periodic or quasi-periodic one, that was subjected to the front in the system. Worth to mention that the spurious drift of the "backward" running ($s_0 < 0$) fronts practically disappeared in both cases of the periodic and quasi-periodic ac forces, in the whole interval of the driving amplitudes f_a (see curves P_3 and Q_3 in Figure 26).

Another important outcome is a close proximity of both the actual, numerically found $\rho - f_a$ dependences being derived by the governing equation (58), and those derivable analytically by the speed equation (82). The solid curves show numerically found $\rho - f_a$ dependences and those being derived analytically are presented by the dashed curves in Figure 25. It should be noted that both $\rho - f_a$ dependences discussed practically coincided if the frequency of the fastest (super-harmonic) mode of the oscillatory forces used was much lesser if compared to the characteristic relaxation rate of the system, namely, when the criterion of the slow driving, $\mu\omega\tau_R << 1$, was satisfied. Consequently, the oscillatory forces that have been used in the numerical derivation of the discussed dependences were taken slow enough (see the figure caption). Finally, both the numerically found $\rho - f_a$ characteristics and those derivable analytically, within the adiabatic (quasi-stationary) approximation discussed practically coincide, in both cases of the periodically and quasi-periodically forced BFs.

In summary, the temporally irregular oscillations of the unbiased oscillatory forcing shrink the spurious drift of BF: the performance of ratchet-like shuttling of BFs is much lesser pronounced with the quasi-periodic, temporally irregular ac forcing if compared to that derivable by the rigorously periodic ac force. Next section deals with the ratchet-like shuttling of the quasi-

periodically forced BFs being under the action of the fast, rapidly oscillating forces.

4.2.2 Self-ordered front under rapidly oscillatory force

Turning to the higher driving frequencies ω, the average $\rho-\omega$ characteristics that describe the dependence of the acceleration factor versus the frequency ω of the basic mode of the oscillatory forces used are presented in Figure 27 and Figure 28. Results presented in Figure 27 are derived by use of the symmetrical rate function and the other case of the asymmetrical rate function is presented in Figure 28. The solid curves (labeled by Q) show the $\rho-\omega$ dependences being derived by the quasi-periodic forcing and the other case of the periodically forced BFs is presented by the dashed curves (labeled by P) in both figures. One can see that the presented $\rho-\omega$ dependences derivable by both oscillatory forces are similarly shaped: the acceleration factor progressively decreases with the increasing frequency ω, in both cases of the symmetrical and asymmetrical rate functions. Nevertheless, the "efficiency" of both drivers, more specifically, the acceleration factors ρ derivable by both oscillatory forces, the periodic and quasi-periodic one, notably differ. Namely, they deviate more significantly from each other in the low-frequency range, $\omega<(\mu\tau_R)^{-1}$, only: the performance of the ratchet-like shuttling of BF is much more pronounced with the periodic forcing, in both cases of the symmetrical and asymmetrical rate functions (compare the solid and dashed curves in both Figure 27 and Figure 28).

In case of higher frequencies ω, the acceleration factors ρ drivable by both oscillatory forces are close to each other, they practically coincide. Such a dissimilar behavior of both the periodically and quasi-periodically forced BFs within low and high frequency intervals discussed may be attributed to the retardation effects in the front dynamics. A close proximity of the discussed $\rho-\omega$ dependences in the frequency domain $\omega>(\mu\tau_R)^{-1}$ demonstrates that the fastest (super-harmonic) mode of both forcing functions $f_P(t)$ and $f_Q(t)$ is "passive", in terms of the spurious drift discussed, i.e., it contributes to the

directed net motion of the BF only very insignificantly. To be more specific, the contribution of the super-harmonic mode of both oscillatory forcing functions to the spurious drift of BF is insignificant if the frequency of the super-harmonic mode, $\mu\omega$, exceeds the characteristic relaxation rate of the system (for related studies see [57, 59]). Namely, when the relation $\mu\omega \geq \tau_R^{-1}$ is satisfied, i.e., the peculiarities of the ratchet-like transport derivable by both oscillatory forces discussed will practically coincide.

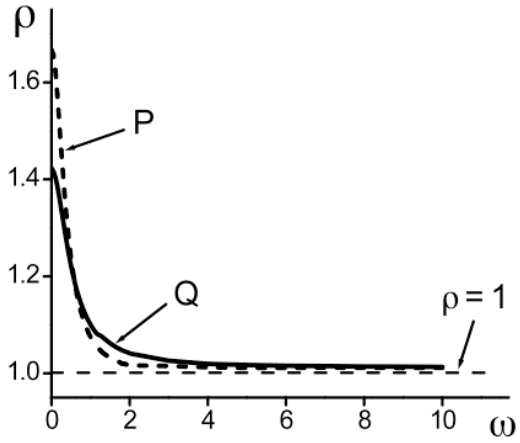

Figure 27. The acceleration factors of both the periodically and quasi-periodically driven BFs versus the frequency of the fundamental mode of the forcing functions $f_P(t)$ and $f_Q(t)$ (shown by the dashed (P) and the solid (Q) curves, respectively). The characteristic parameters of the symmetrical rate function are as follows: $\alpha_1 = \alpha_3 = 1.0$, $\alpha_2 = 5.0$ and $h_R \approx 1.05$. The rest of the parameters are: $s_0 \approx 0.009$, $f_a = 0.9 f_{Mx}$ and $\tau_R = 1.0$.

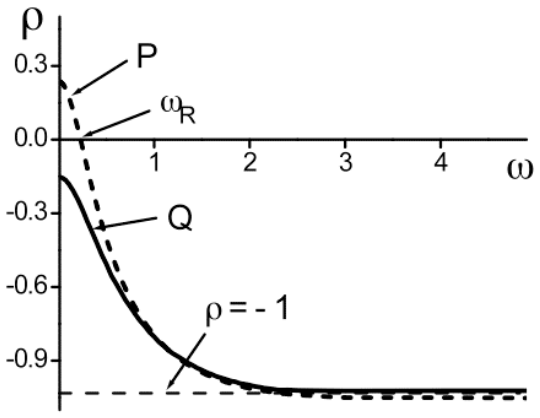

Figure 28. The same as in Figure 27 but for the other case of the asymmetrical rate function. The frequency of the ac force, $\omega = \omega_R \approx 0.23$, at which the reversal of the directed net motion of the periodically driven BF takes place is pointed by the arrow. Parameter values of the rate function are as follows: $\alpha_1 = 5.0$, $\alpha_2 = 3.0$, $\alpha_3 = 1.0$, $h_0 \approx 1.58$ and $h_R \approx 1.44$. The rest of the parameters are: $s_0 \approx -0.024$, $f_a = 0.9 f_{Mx}$ and $\tau_R = 1.0$.

The mean drift velocity of the ac driven BF may be controllable by adjusting both the amplitude f_a and the frequency ω of the oscillatory forcing. As a result, the occurrence/vanishing of the reversals should be sensitive to both parameters discussed. Regretfully, the rigorous criteria for the existence (occurrence/vanishing) of the reversals are lacking but, generally speaking, the reversal implies that the average characteristic of the ac driven BF, either $\rho - \omega$ or $\rho - f_a$, has at least one null (zero-point). In particular, the average $\rho - \omega$ characteristics shown in Figure 28 demonstrate that the reversal of the

unforced dc motion of BF takes place with the periodic ac force only; the progressively decreasing (decelerated) dc drift of the quasi-periodically driven BF is observed with the increasing frequency ω. This dissimilar behavior of both the periodically and quasi-periodically forced BFs is observed in the low-frequency domain, $\omega < (\mu\tau_R)^{-1}$, by tuning the oscillatory frequency ω. Finally, the reversal of the periodically forced BF takes place when the system satisfies the "critical" frequency, $\omega = \omega_R$, namely, the null-point of the average $\rho - \omega$ characteristic (ω_R is pointed by arrow in Figure 28).

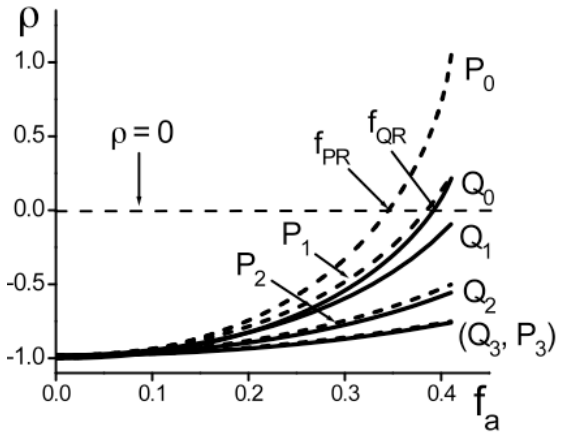

Figure 29. The acceleration factor of the ac driven front versus the amplitude of the oscillatory force. The average $\rho - f_a$ characteristics of the periodically and quasi-periodically forced BFs are presented by the dashed (P_j) and the solid (Q_j) curves, respectively. The parameters of the asymmetrical rate function are as follows: $\alpha_1 = 5.0$, $\alpha_2 = 3.0$, $\alpha_3 = 1.0$, $h_0 \approx 1.58$ and $h_R \approx 1.44$. The rest of the parameters are: $s_0 \approx 0.009$ and $\tau_R = 1$. The frequencies ω of the oscillatory forces being related to the separate pairs of the curves labeled by (P_0, Q_0), (P_1, Q_1), (P_2, Q_2) and (P_3, Q_3) are as follows: $\omega\tau_R$=0.01, 0.30, 0.70, and 1.00, respectively. Notice that the average $\rho - f_a$ characteristics being derived by both the periodic and quasi-periodic forcing functions that satisfy the relation $\mu\omega\tau_R \geq 1$ are very close to each other (compare the interrelated curves labeled by (P_2, Q_2) and (P_3, Q_3), respectively).

The average $\rho - f_a$ characteristics being derived at the different frequencies ω of the oscillatory forces used confirm this prediction; these are shown in Figure 29. One can see that the presented $\rho - f_a$ dependences are decreasingly sloped with the frequency ω of the oscillatory force being increased (compare the curves labeled by (P_0,Q_0), (P_1,Q_1), (P_2,Q_2) and (P_3,Q_3) in Figure 29). This behavior can be attributed to the retardation effects in the front dynamics that shrink the spurious drift of BFs. More specifically, the lag time between the ac

force $f(t)$ and the speed function $s(t)$ of the ac driven BF increases with the increasing frequency of the ac forcing, as a consequence, the average $\rho - f_a$ characteristics of the spurious drift of BFs become more and more flattened with the oscillatory frequency of the ac force being increased. The curves (P_0,Q_0) and (P_1,Q_1) in Figure 29 are more steeply sloped when the slow oscillatory forces satisfying the relation $\omega < \tau_R^{-1}$. Furthermore, the reversal behavior of the ac driven BFs is observed in the case of the slow oscillatory forces only, when the retardation effects in the front dynamics are insignificant. The "critical" amplitudes f_{PR} and f_{QR} at which the reversals of both the periodically and quasi-periodically driven BFs take place are pointed by arrows in the Figure 29. It should be noted that the average $\rho - f_a$ characteristics shown by curves P_0 and Q_0 are in accord with the previous findings demonstrated in Figure 26 and Figure 28. Results show that BFs propagate, on average, in the opposite directions depending on the amplitude f_a of the oscillatory forces, the periodic and quasi-periodic one, taken within the interval $[f_{PR}, f_{QR}]$.

4.2.3 Summary

In this section the periodic and quasi-periodic ac forces acting on the front in the system were approximated by the bi-harmonic, temporally irregular forcing function being a superposition of the single-harmonic components (the Fourier modes) that were characterized by the incommensurate, rationally independent frequencies. By considering the response of the self-ordered front to the bi-harmonic oscillatory forces, both the periodic and quasi-periodic one, the following conclusions were made:

- The temporally irregular oscillations of the unbiased oscillatory forcing shrink the spurious drift of BFs; the performance of the ratchet-like shuttling of the quasi-periodically forced BFs is much lesser pronounced if compared to that derivable by the rigorously periodic ac force, in both cases of the symmetrical and asymmetrical rate functions satisfying different symmetry.

- The average characteristics of the ratchet-like transport derivable by the different oscillatory forces, the periodic and quasi-periodic one, deviate more significantly from each other in the low-frequency range of the oscillatory forces, when the frequency of the super-harmonic (fastest) mode of the oscillatory forces used is lesser if compared to the characteristic relaxation rate of the system. In contrast, at the higher frequencies of the ac forces, beyond the low-frequency domain discussed, the average characteristics of the ratchet-like transport of both the periodically and quasi-periodically forced BFs practically coincide.
- Quite different, dissimilar reversal behavior of the unforced dc motion of both the periodically and quasi-periodically driven BFs is observed (identified) in the low-frequency domain. Reversals discussed do not occur when temporarily irregular forcing is applied.

4.3 Quasi-periodically forced fronts: multi-harmonic forcing

In this section a new possibilities of controlling the directed net motion of BFs by use of the quasi-periodic zero-average forces of the different spectral content are investigated. The oscillatory forces acting on the front in the system are approximated by the multi-harmonic forcing function (67) being a superposition of the single-harmonic components of the different frequencies, either commensurate or incommensurable ones. The bi-, tri-, tetra-, and penta-harmonic forcing functions, both the quasi-periodic $f_Q(t)$ and periodic $f_P(t)$ ones, are used to study the "efficiency" in terms of the spurious drift of the driven BFs. The objective is to investigate what happens with the quasi-periodically forced BF, by gradually extending the frequency spectrum of the incommensurable frequency modes of the ac forcing $f(t)$ acting of the front in the system. Furthermore, it is not clear whether the quasi-periodically or periodically forced BFs being subjected to the oscillatory forces of the similar spectral content can provide the better performance of the ratchet-like shuttling. For this reason, the acceleration factor $\rho := |s_0|^{-1} v$, which denotes the

relative increase of the mean drift velocity v of the ac driven of BF, is used to evaluate the "efficiency" of the oscillatory forces of zero-time average.

The characteristics of the acceleration factor ρ of the ac driven front versus the amplitude f_a of the ac force are presented in Figure 30. All average $\rho - f_a$ characteristics are found numerically using the governing equation (58) with the multi-harmonic forcing functions $f_Q(t)$ and $f_P(t)$ of the similar spectral content. The curves labeled by P_n and Q_n refer to the periodically and quasi-periodically forced BFs, respectively, and the subscripts 2, 3, 4 and 5 denote the bi-, tri- tetra-, and penta-harmonic forcing functions, respectively. The average $\rho - f_a$ characteristics derivable by the symmetrical rate function (48) demonstrate that both the periodically and quasi-periodically forced BFs exhibit quite similar behavior when gradually extending the frequency spectrum of the oscillatory ac forcing. Indeed, one can see that the presented $\rho - f_a$ dependences of the slow oscillatory forces satisfying the relation $\mu\omega\tau_R << 1$ are getting more flattened with every additional single-harmonic component of the different frequency (compare the corresponding $\rho - f_a$ dependencies of the different frequency spectrum in Figure 30).

Furthermore, the presented $\rho - f_a$ dependences evidently demonstrate that the performance of the ratchet-like shuttling of BFs is much lesser pronounced with the quasi-periodic, temporally irregular ac forcing, if compared to the periodic one (compare the corresponding $\rho - f_a$ dependencies in Figure 30). In addition, the numerically obtained results demonstrate that the ratchet-like shuttling of the quasi-periodically forced BF, being induced by penta-harmonic forcing function, practically disappears in the whole interval of the driving amplitudes f_a; (see curve Q_5 in Figure 30). In other words, the mean drift velocity v of the BF driven by the quasi-periodically force with the highest frequency spectrum becomes very close to that of free, unperturbed BF, s_0. In contrast, the periodic penta-harmonic ac driver demonstrates a relatively high "efficiency" (see curve P_5).

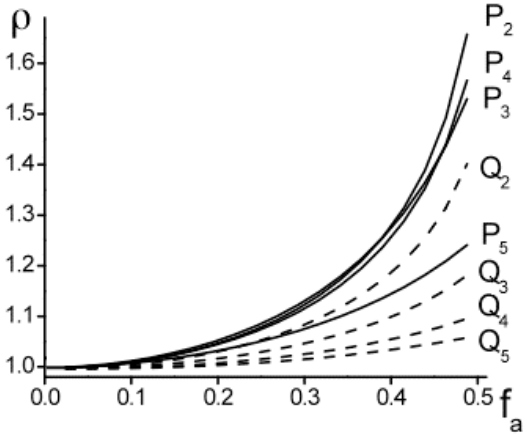

Figure 30. The acceleration factor ρ of the ac driven front versus the amplitude f_a of the low-frequency zero-mean ac forces satisfying the relation $\omega_{Mx} << \tau_R^{-1}$. The average characteristics that are derived by both the quasi-periodic and periodic ac forces are presented by the solid (labeled by P_n) and dashed curves (labeled by Q_n) curves, respectively; the subscripts 2, 3, 4, and 5 denote the bi-, tri-, tetra-, and penta-harmonic forcing functions, respectively. The characteristic parameters of the rate function are: $\alpha_1 = \alpha_3 = 1.0$, $\alpha_2 = 3.0$ and $h_R = 1.05$. The rest of the parameters are as follows: $s_0 \approx 0.009$, $\tau_R = 1.0$, and $\omega\tau_R = 0.01$. Notice, the unforced dc drift of BF under the penta-harmonic oscillatory force exhibiting the temporally irregular behavior is practically disappeared in the whole interval of the driving amplitudes f_a (see curve Q_5).

The average $\rho - \omega$ characteristics being derived by use of the quasi-periodic forces $f_Q(t)$ describe the dependence of the acceleration factor versus the frequency ω of the basic mode of the multi-harmonic functions are presented in Figure 31. The curves labeled by Q_2, Q_3, Q_3 and Q_5 refer to the bi-, tri-, tetra-, and penta-harmonic functions $f_Q(t)$, respectively. One can see that the maximal acceleration factor, the maximal shift of the mean drift velocity of the quasi-periodically forced BF is achieved in the low-frequency domain satisfying the relation $\omega_{Max} << \tau_R^{-1}$ where the denotation, $\omega_{Max} = \max\{\mu_j\}\omega$, stands for the largest frequency of the "fastest" super-harmonic mode of the ac forcing. Quite different situation is in the high frequency range, $\omega \geq \tau_R^{-1}$, where the acceleration factors ρ rapidly decrease with the increasing frequency ω; ratchet-like shuttling of the self-ordered fronts practically disappear. Furthermore, the "efficiency" of the quasi-periodic ac driver rapidly decreases by extending the frequency spectrum of the oscillatory forcing (compare the separate curves in Figure 31). As a result, the optimal, effective controlling the

directed net motion of BFs by use of the temporally irregular ac forces is achieved with the slow oscillatory forces that are characterized by the narrowly spaced (bi-harmonic) frequency spectrum.

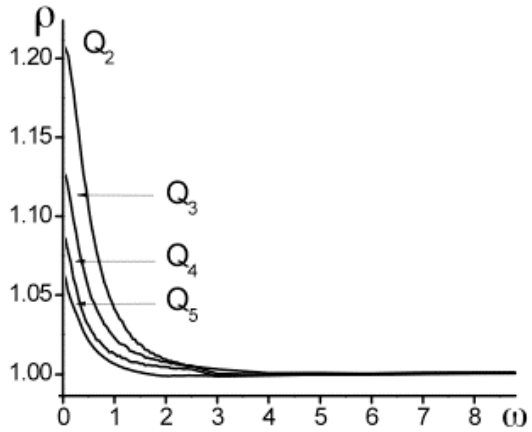

Figure 31. The acceleration factor of the quasi-periodically forced BFs versus the frequency of the fundamental mode of the quasi-periodic zero-mean valued ac forces $f_Q(t)$. The curves labeled by Q_2, Q_3, Q_4, and Q_5, refer to the bi-, tri-, tetra-, and penta-harmonic forcing functions, respectively. The characteristic parameters of the rate function are as follows: $\alpha_1 = \alpha_3 = 1.0$, $\alpha_2 = 3.0$ and $h_R \approx 1.05$. The rest of the parameters are: $s_0 \approx 0.0108$, $f_a = 0.8 f_{Mx}$ and $\tau_R = 1.0$. Notice how curves get more gently sloped with an increase of frequency spectrum.

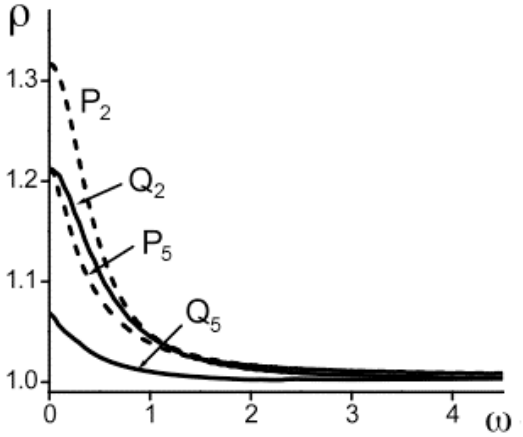

Figure 32. The same as in Figure 31, but for the quasi-periodic and periodic ac forces that are shown by the solid (labeled by Q) and dashed curves (labeled by P) curves, respectively; the subscripts 2 and 5 refer to the bi- and penta-harmonic forcing functions, respectively. The amplitude of the oscillatory forces used was taken as follows, $f_a = 0.8 f_{Mx}$.

The average $\rho - \omega$ characteristics derivable by both cases of the periodic and quasi-periodic forces using the bi-harmonic and penta-harmonic forcing functions are presented in Figure 32. As previously, the labels P and Q refer to the periodic and quasi-periodic forcing functions $f_Q(t)$ and $f_P(t)$, respectively, and the subscripts 2 and 5 denote the bi- and penta-harmonic forcing functions, respectively. One can see that the performance of the ratchet-like shuttling of BF is much less pronounced with the quasi-periodic, temporally irregular ac forcing in the low-frequency domain satisfying the relation $\omega_{Max} << \tau_R^{-1}$ (compare the solid and dashed curves in Figure 32). On the other hand, the acceleration factors derivable by both oscillatory forces practically coincide at the higher frequencies, $\omega \geq \tau_R^{-1}$, far beyond the low-

frequency interval discussed. Such a dissimilar behavior of both the periodically and quasi-periodically forced BFs within two different frequency intervals discussed may be attributed to the retardation effects in the front dynamics. In short, the numerically obtained results confirm that the spurious drift of the randomly "wandering" BF shrinks and are in reasonable agreement with the previous results being derived in case of bi-harmonic forcing function.

4.3.1 Summary

The quasi-periodic and periodic ac forces of zero-time average acting on the front in the system were approximated by the multi-harmonic forcing function being a linear combination (sum) of the single-harmonic components with rational and irrational numbers, respectively. By numerically simulating the drift motion of the ac driven BF under the multi-harmonic ac forcing of the similar spectral content, both the quasi-periodic and periodic one, the following conclusions were made:

- The performance of the ratchet-like shuttling is much lesser pronounced with the quasi-periodic, temporally irregular ac forces, if compared to the periodic ones.
- The directed transport of the quasi-periodically forced BF very rapidly decreases by extending the frequency spectrum of the incommensurable frequency modes of the ac forcing.
- The optimal, effective controlling the directed net motion of BFs by use of the quasi-periodic zero-average forces is achieved in the low-frequency domain of the ac forces. In contrast, the average characteristics show that the ratchet-like transport of both the periodically and quasi-periodically forced BFs practically disappears at the high-frequency domain of the ac forces.

4.4 Fronts driven by bounded noise

The noise-induced drift of BFs under the bounded noise forces (68) is investigated in this section. Previous investigations being performed using perturbation techniques demonstrated that the unforced dc drift of the "randomly wondering" BFs under the weak, low-intensity noisy forces was sensitive to the spectral content of the forcing (noise spectrum) [8, 10, 12]. It was shown in [12] that the white (uncorrelated) Gaussian noise is not capable to induce the directed net motion of BF. In particular, the spurious drift of BFs under weak noisy forces disappeared if the noisy force was Gaussian and delta correlated. Obviously, the perturbation theory fits well only in the limited case of the weak forcing. Therefore, in this research numerical simulations are employed to study the noise-induced drift of BFs at the higher levels of the noise, beyond the perturbative approaches discussed. The focus of the section is on how noise-assisted propagation of BFs under the bounded noise forces of zero-time average reacts to the gradually increasing intensity of the noise. More specifically, higher levels of noise are achieved by gradually increasing value of the maximal frequency ω_{Max} of the bounded noise function (68). As before, the same acceleration factor $\rho := |s_0|^{-1} v$ is used to measure the "efficiency" of the bounded noise, in terms of the spurious drift of the BF.

The average characteristics of the acceleration factor ρ versus the standard deviation σ of zero-mean bounded noise forces are presented in Figure 33. All $\rho - \sigma$ dependences in the figure are derived using forcing function (68) without the phase shift, $\varphi_n = 0$, while the random frequency ω_n being uniformly distributed in the interval $[\omega_m, \omega_M]$. The same minimum frequency, $\omega_m = 0.005\tau_R^{-1}$, of the slowest mode of the forcing function (68) has been taken for all calculations. In addition, all force realizations have the same distribution density $\gamma_\omega = 155$ in the frequency spectrum $[\omega_m, \omega_M]$. One can see that the presented $\rho - \sigma$ dependencies being derived by bounded noise are getting much more flattened with an increase of frequency spectrum, maximal

frequency ω_{Max} (compare the corresponding $\rho-\sigma$ dependencies in Figure 33). The maximal acceleration factor $\rho_{\max} \equiv \rho(\sigma_{Max})$ of the noise-induced drift of BF has the highest value, $\rho_{\max}=1.155$, when the frequency spectrum is very narrow, $\omega_m = 0.05\tau_R^{-1}$, and the level of noise is relatively low (see curve 1 in Figure 33). In contrast, the contribution of the bounded noise with the widest frequency spectrum, $\omega_m = 5\tau_R^{-1}$, to the spurious drift discussed is very small, only insignificant; the noise-assisted propagation of the BF being induced by bounded noise forcing function of the highest level of noise (the highest number of modes, $N=774$) practically disappears in the whole interval of the standard deviation σ of the driving force (see curve 5 in Figure 33).

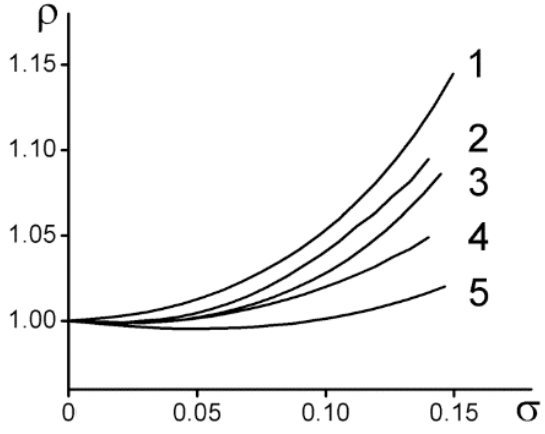

Figure 33. The acceleration factor of the noise-assisted propagation of BFs versus the standard deviation of zero-mean bounded noise forces without phase shift, $\varphi_n = 0$. The maximal frequencies ω_{Max} and number of modes N of the ac forces being related to the separate curves are labeled as follows: (curve 1) $\omega_{Max}\tau_R = 0.05$, $N=7$; (curve 2) $\omega_{Max}\tau_R = 0.3$, $N=46$; (curve 3) $\omega_{Max}\tau_R = 0.5$, $N=77$; (curve 4) $\omega_{Max}\tau_R = 0.8$, $N=123$; (curve 5) $\omega_{Max}\tau_R = 5.0$, $N=774$. The distribution density stays the same: $\gamma_\omega = 155$. The characteristic parameters of the rate function are as follows: $\alpha_1 = \alpha_3 = 1.0$, $\alpha_2 = 5.0$ and $h_R \approx 1.05$. The rest of the parameters are: $\omega_m = 0.005\tau_R^{-1}$, $s_0 \approx 0.0094$ and $\tau_R = 1.0$. Notice how curves get more gently sloped with an increase of frequency spectrum.

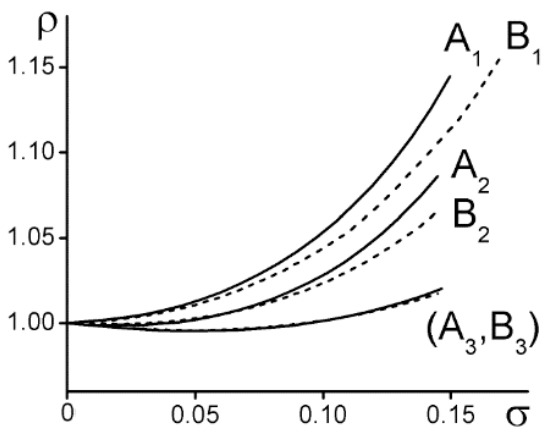

Figure 34. The average $\rho-\sigma$ characteristics derived by bounded noise with the random phase shift φ_n being uniformly distributed in the interval $[0, 2\pi]$ and without phase shift, $\varphi_n = 0$, are presented by the dashed (B_j) and the solid (A_j) curves, respectively. The parameters of the rate function are as follows: $\alpha_1 = \alpha_3 = 1.0$, $\alpha_2 = 5.0$ and $h_R \approx 1.05$. The rest of the parameters are: $\omega_m = 0.005\tau_R^{-1}$, $s_0 \approx 0.0094$, $\tau_R = 1.0$ and $\gamma_\omega = 155$. The maximal frequencies ω_{Max} of the bounded noise forces being related to the separate pairs of the curves labeled by (A_1, B_1), (A_2, B_2) and (A_3, B_3) are as follows: $\omega_{Max}\tau_R$=0.05, 0.5 and 5.0, respectively. Notice that the average $\rho-\sigma$ characteristics being derived by both types of forcing functions that satisfy the relation $\mu\omega\tau_R \geq 1$ are very close to each other (compare the interrelated curves (A_3, B_3)).

Quite similar situation is observed when the random phase shift φ_n of the forcing function (68) is applied. The average $\rho - \sigma$ characteristics of the noise-induced drift of the BF driven by bounded noise with the random phase shift φ_n being uniformly distributed in the interval $[0, 2\pi]$ are presented by dashed curves (B_j) in the Figure 34. One can see that the presented $\rho - \sigma$ dependences are decreasingly sloped with the increasing intensity of the noise in frequency of forcing function. Nevertheless, the performance of the ratchet-like shuttling discussed derivable by bounded noise with and without phase shift φ_n notably differs; the unforced dc drift of BFs is much lesser pronounced with the random phase shift $\varphi_n \in [0, 2\pi]$, as follows from the direct numerical calculations being performed with the bounded noise forcing functions (68) of the same spectral content (compare the solid and dashed curves in Figure 34). In addition, the average $\rho - \sigma$ characteristics of the noise-induced drift of the BF driven by bounded noise with and without phase shift φ_n practically coincide in the highest noise spectrum, $\omega_{Max}\tau_R >> 1$ (see curves (A_3, B_3) the Figure 34).

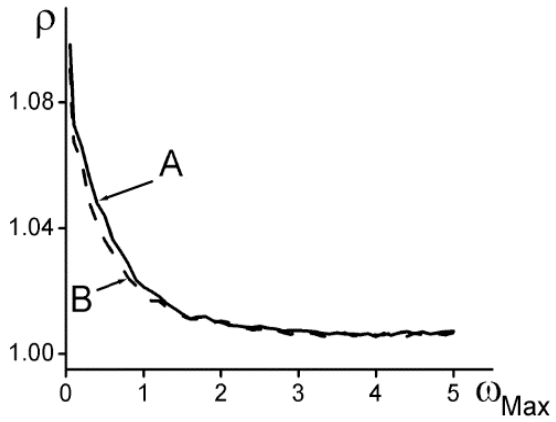

Figure 35. The acceleration factor ρ of the ac driven front versus the maximal frequency ω_{Max} of the zero-mean bounded noise forces. The average characteristics that are derived by the forcing function without the phase shift, $\varphi_n = 0$, are shown by the solid curve (labeled by A) and with the random phase shift φ_n being uniformly distributed in the interval $[0, 2\pi]$ are shown by the dashed curve (labeled by B). The parameters of the rate function are as follows: $\alpha_1 = \alpha_3 = 1.0$, $\alpha_2 = 5.0$ and $h_R \approx 1.05$. The rest of the parameters are: $\omega_m = 0.005\tau_R^{-1}$, $s_0 \approx 0.0094$, $\tau_R = 1.0$ and $\gamma_\omega = 155$. The standard deviation of the oscillatory forces used was taken as follows, $\sigma = 0.8\sigma_{Max}$.

The average $\rho - \omega_{Max}$ characteristics that describe the dependence of the acceleration factor versus the maximal (fastest) frequency ω of zero-mean bounded noise forces used are presented in Figure 35. As previously, the labels A and B refer to the bounded noise forcing function with and without phase shift φ_n, respectively. One can see that the presented $\rho - \omega_{Max}$ dependences derivable in both cases are similarly shaped: the acceleration factor progressively decreases with the increasing frequency spectrum (noise spectrum). Nevertheless, the "efficiency" of both drivers deviate more from each other in the narrow spectral content of the forcing, $\omega_{Max} < \tau_R^{-1}$, only: the performance of the noise-induced drift of the BF is much more noticeable when the random phase shift φ_n of the forcing function is not applied, $\varphi_n = 0$ (compare the solid and dashed curves in Figure 35). In contrast, the acceleration factors ρ drivable by both bounded noise forces are close to each other, they practically coincide in wide frequency spectrum, $\omega_M >> \tau_R^{-1}$; the mean drift velocity of the ac driven front rapidly decreases by extending the frequency spectrum (noise spectrum) of the ac forcing. As a result, the noise-induced drift of BFs practically disappears when the intensity of the noise increases.

4.4.1 Summary

The possibilities of controlling the directed net motion of the ac driven BFs by use of the zero-mean valued bounded noise forces have been investigated. By numerically simulating the noise-induced drift of BFs under the strong, high-intensity noisy forces of the similar (close) spectral content, the following conclusions were made:

- The performance of the ratchet-like shuttling is much lesser pronounced with the random phase shift of bounded noise forces, if compared to the forces without phase shift.
- The noise-induced drift of the BF is very sensitive to the spectral content of the forcing (noise spectrum); the noise-assisted propagation

of BFs very rapidly decreases as the intensity of the noise in frequency increases.

- The effective controlling the directed net motion of BFs by use of the zero-average bounded noise forces is achieved in the narrow spectral content of the forcing. In contrast, the noise-induced drift of BFs practically disappears at the wide spectral content of the ac forces.

5. Conclusions

The spatio-temporal control of the bistable fronts joining two states of the different stability in a bistable system of the reaction-diffusion type has been studied using computer modelling. The following conclusions can be drawn from the present research:

1) The constructed mathematical and numerical models can be used for investigations of the self-ordered BF under deterministic and noisy oscillatory fields of zero-time average. Both numerically and analytically derived results coincide well.
2) The optimal, more effective controlling of the directed net motion of BFs is achievable in the low-frequency domain of the oscillatory force, by the slow (quasi-stationary) ac drive. The retardation effects in the front dynamics, that become more pronounced in the high-frequency range of the zero-mean ac forces, shrink the spurious drift of the front, in both cases of the symmetrical and asymmetrical rate functions satisfying the different R-u symmetry.
3) The characteristic relaxation time, that describes the rate of the transient processes in a bistable system, derivable analytically, within the perturbation theory is adequate enough even in case of the strong forcing, as follows from the numerical simulations.
4) The oscillatory unbiased forces exhibiting the temporally irregular behavior, both the deterministic (quasi-periodic) and noisy ones, are much lesser effective in terms of the ratchet-like shuttling of BFs if compared to periodic ones.
5) The temporally irregular ac forces with a broader spectral content, both the deterministic (quasi-periodic) and noisy ones, result in much lower performance of the ratchet-like shuttling of BFs. The directed net motion of the ac driven BF rapidly decreases by gradually extending the frequency spectrum of the incommensurable frequency modes of the oscillating force.

6. References

1. P. Reimann, Brownian motors: Noisy transport far from equilibrium, *Phys. Rep.*, **361**, pp. 57–265, 2002.
2. A. S. Mikhailov, L. Schimansky-Geier, and W. Ebeling, Stochastic motion of the propagating front in bistable media, *Phys. Lett. A*, **96**, pp. 453–456, 1983.
3. F. J. Cao, E. Zamora-Sillero, and N. R. Quintero, Domain wall dynamics in expanding spaces, *Physical Review E*, **73**, pp. 056603, 2006.
4. D. H. Sattinger, On the stability of waves of nonlinear parabolic systems, *Adv. Math.*, **22**, pp. 312–355, 1976.
5. R. Bakanas, Traveling fronts in a piecewise-linear bistable system, *Nonlinearity*, **16**, pp. 313–325, 2003.
6. J. Armero, J. M. Sancho, J. Casademunt, A. M. Lacasta, L. Ramírez-Piscina, and F. Sagués, External fluctuations in front propagation, *Phys. Rev. Lett.*, **76**, pp. 3045, 1996.
7. J.M. Sancho M.A. Santos, Front dynamics in the presence of spatiotemporal structured noises, *Phys. Rev. E*, **64**, pp. 016129, 2001.
8. R. Landauer M. Büttiker, Nucleation theory of overdamped soliton motion, *Phys. Rev. A*, **23**, pp. 1397, 1981.
9. J.M. Sancho and A. Sanchez, External fluctuations in front dynamics with inertia: The overdamped limit, *Eur. Phys. J.*, **16**(1), pp. 127-131, 2000.
10. D.J. Kaup, Thermal corrections to overdamped soliton motion, *Phys. Rev. B*, **27**(11), pp. 6787-6795, 1983.
11. L. Schimansky-Geier and Ch. Zulicke, Kink propagation induced by multiplicative noise, *Z. Phys. B Con. Mat.*, **82**, pp. 157–162, 1991.
12. F. Marchesoni, Thermal Ratchets in 1+1 Dimensions, *Phys. Rev. Lett.*, **77**, pp. 2364–2367, 1996.
13. N.R. Quintero, A. Sanchez, and F.G. Mertens, Overdamped sine-Gordon kink in a thermal bath, *Phys. Rev. E*, **60**(1), pp. 222–230, 1999.
14. M.G. Clerc, C. Falconi, and E. Tirapegui, Additive noise induces front propagation, *Phys. Rev. Lett.*, **94**, pp. 148302-(1–4), 2005.
15. R. Bakanas, Unidirectional drift of fronts under zero-mean force and broken symmetries of the rate function, *Phys. Rev. E*, **69**(1), pp. 016103-(1–10), 2004.
16. R. Bakanas, Unidirectional drift of bistable front under asymmetrically oscillating zero-mean force, *Phys. Rev. E*, **71**, pp. 026201-(1–12), 2005.

17. R. Bakanas, Rectified oscillatory motion of the self-ordered front under zero-mean ac force: Role of symmetry of the rate function, *Phys. Rev. E*, **78**(4), 046202, 2008.

18. F. G. Bass and R. Bakanas, Fronts in a continuous bistable system under periodically oscillating forcing, *Europhys. Lett.*, **53**(4), pp. 444-450, 2001.

19. I. Zapata, R. Bartussek, F. Sols, and P. Hänggi, Voltage rectification by a SQUID ratchet, *Phys. Rev. Lett.*, **77**, pp. 2292–2295, 1996.

20. M. Beck, E. Goldobin, M. Neuhaus, M. Siegel, R. Kleiner, and D. Koelle, High-Efficiency Deterministic Josephson Vortex Ratchet, *Phys. Rev. Lett.*, **95**(9), pp. 090603, 2005.

21. M.V. Fistul, E. Goldobin, and A.V. Ustinov, ac-induced damping of a fluxon in a long Josephson junction, *Phys. Rev. B*, **64**, pp. 092501, 2001.

22. A. V. Ustinov, C. Coqui, A. Kemp, Y. Zolotaryuk, and M. Salerno, Ratchetlike Dynamics of Fluxons in Annular Josephson Junctions Driven by Biharmonic Microwave Fields, *Phys. Rev. Lett.*, **93**, pp. 087001, 2004.

23. F. Falo, P.J. Martínez, J.J. Mazo, T.P. Orlando, K. Segall, and E. Trías, Fluxon ratchet potentials in superconducting circuits, *Applied Physics A: Materials Science & Processing*, **75**(2), pp. 263-269, 2002.

24. R. Besseling, P.H. Kes, T. Droese, and V.M. Vinokur, Depinning and dynamics of vortices confined in mesoscopic flow channels, *New Journal of Physics*, **7**(71), 2005.

25. F. Nori and S. Savel'ev, Controlling vortex motion and vortex kinetic friction, *Physica C*, **437**, pp. 226-229, 2006.

26. M. Löcher, D. Cigna, and E. R. Hunt, Noise sustained propagation of a signal in coupled bistable electronic elements, *Phys. Rev. Lett.*, **80**, pp. 5212, 1998.

27. M. Löcher, N. Chatterjee, F. Marchesoni, W. L. Ditto, and E. R. Hunt, Noise sustained propagation: Local versus global noise, *Phys. Rev. E*, **61**, pp. 4954, 2000.

28. M. O. Magnasco, Forced thermal ratchets, *Phys. Rev. Lett.*, **71**(10), pp. 1477–1481, 1993.

29. J.F. Chauwin, A. Ajdari, and J. Prost, Force-Free Motion in Asymmetric Structures: a Mechanism without Diffusive Steps, *Europhys. Lett.*, **27**(6), pp. 421-426, 1994.

30. R. D. Astumian and M. Bier, Fluctuation Driven Ratchets: Molecular Motors, *Physical Review Letters*, **72**(11), pp. 1766-1769, 1993.

31. C. R. Doering, W. Horsthemke, and J. Riordan, Nonequilibrium Fluctuation-Induced Transport, *Physical Review Letters*, **72**(19), pp. 2984-2987, 1994.

32. M. von Smoluchowski, Experimentell nachweisbare, der Ublichen Thermodynamik widersprechende Molekularphenomene, *Physik Zeitschr*, **13**, pp. 1069–1080, 1912.

33. R.P. Feynman, R.B. Leighton, and M. Sands, *The Feynman Lectures on Physics*. Vol. 1, (Chapter 46), Addison-Wesley, Reading, MA, 1963.

34. J. C. Maxwell, *Theory of Heat.*, Dover Publications, Inc.1871.

35. P. Reimann and P. Hänggi, Introduction to the physics of Brownian motors, *App. Phys. A*, **75**(2), pp. 169-178, 2002.

36. A. M. Jayannavar, Inhomogeneous systems and their rectification properties, Preprint [e-print], cond-mat/0107079, pp. 1-40, 2001.

37. H.B. Callen and T.A. Welton, Irreversibility and generalized noise, *Phys. Rev.*, **83**(1), pp. 34–40, 1951.

38. M. Büttiker, Transport as a consequence of state-dependent diffusion, *Z. Phys. B* **68**(2-3), pp. 161-167, 1987.

39. R. Landauer, Motion out of noisy states, *J. Stat. Phys*, **53**, pp. 233-48, 1988.

40. F. Jülicher, A. Ajdari, and J. Prost, Modeling molecular motors, *Rev. Mod. Phys.*, **69**, pp. 1269–1282, 1997.

41. P. Hänggi, F. Marchesoni, and F. Nori, Brownian motors, *Annalen der Physik*, **14**(1-3), pp. 51–70, 2005.

42. P. Hänggi and F. Marchesoni, Artificial Brownian motors: Controlling transport on the nanoscale, *Rev. Mod. Phys.*, **81**, pp. 387- 422, 2009.

43. R. D. Astumian and P. Hänggi, Brownian Motors, *Physics Today*, **55**(11), pp. 33–39, 2002.

44. R. Mallik and S. P. Gross, Molecular Motors: Strategies to Get Along, *Current Biology*, **14**, pp. 971-982, 2004.

45. E. Frey, Physics in Cell Biology: On the physics of Biopolymers and Molecular Motors, *ChemPhysChem*, **3**(3), pp. 270–275, 2002.

46. D. Abbott, Overview: unsolved problems of noise and fluctuations, *Chaos*, **11**, pp. 526-538, 2001.

47. A. N. Kolmogorov, I. G. Petrovsky, and N. S. Piskunov, Study of the Difussion Equation with Growth of the Quantity of Matter and its Application to a Biological Problem, *Moskow Univ. Bull. Math*, **Section A. 1**, pp. 1-26, 1937.

48. R. A. Fisher, The wave of advance of advantageous genes, *Annals of Eugenics*, **7**, pp. 355–369, 1937.

49. Ya. B. Zeldovich and D. A. Frank-Kamenetsky, K teorii ravnomernogo rasprostranenia plameni (Toward a theory of uniformly propagating flames)*, Doklady Akademii Nauk SSSR*, **19**, pp. 693–697, 1938.

50. H. G. Purwins, H. U. Bodeker, and Sh Amiranashvili, Dissipative solitons*, Advances in Physics*, **59**(5), pp. 485-701, 2010.

51. A. Scott, *Nonlinear Science: Emergence and Dynamics of Coherent Structure*, 2nd edition, Oxford University Press, Oxford and New York, 2003.

52. R. FitzHugh, Impulses and Physiological States in Theoretical Models of Nerve Membrane*, Biophysical J.* , **1**(6), pp. 445–466, 1961.

53. J. Nagumo, S.Arimoto, and S. Yoshizawa, An active pulse transmission line simulating nerve axon*, Proc. Instit. Radio Eng. Electr.* , **50**, pp. 257-278, 1962.

54. F.G. Bass and R. Bakanas, Propagation of a Gunn wave under the influence of spatially homogeneous random perturbations*, Phys. Lett. A*, **214**, pp. 301-306, 1996.

55. F. Schlögl, C. Escher, and R. Stephen Berry, Fluctuations in the interface between two phases*, Physical Review A*, **27**(5), pp. 2698–2704, 1983.

56. F. Sanchez-Garduno, E. Kappos, and P.K. Maini, A Review of Travelling Wave Solutions of One-dimensional Reaction-Diffusion Equations with Non-Linear Diffusion Term*, FORMA*, **11**, pp. 45-59, 1996.

57. R. Bakanas, F. Ivanauskas, and A. Raguotis, Ratchet-like transport of the self-ordered fronts generated by the similarly shaped rate functions: high-efficiency deterministic front-ratchet*, Phys. Scripta*, **77**, pp. 055003, 2008.

58. A. Raguotis, F. Ivanauskas, and R. Bakanas, Retarded accelerations of the self-organized front: propagation of the bistable front under step-like force*, Lith. J. Phys.*, **45**, pp. 153–160, 2005.

59. A. Raguotis, F. Ivanauskas, and R. Bakanas, Retarding accelerations and ratchet-like transport of the self-ordered front in a bistable system of reaction-diffusion type*, Phys. Scripta*, **74**, pp. 629–637, 2006.

60. S. Flach, Y. Zolotaryuk, A. E. Miroshnichenko, and M. V. Fistul, Broken symmetries and directed collective energy transport in spatially extended systems*, Phys. Rev. Lett.*, **88**, pp. 184101-(1-4), 2002.

61. S. Flach and S. Denisov, Symmetries and transport with quasiperiodic driving*, Acta Physica Polonica B*, **35**(4), pp. 1437-1445, 2004.

62. S. Denisov, S. Flach, A. A. Ovchinnikov, O. Yevtushenko, and Y. Zolotaryuk, Broken space-time symmetries and mechanisms of

rectification of ac fields by nonlinear (non)adiabatic response, *Phys. Rev. E*, **66**, pp. 041104, 2002.

63. J. P. Gleeson, Transport in randomly-fluctuating spatially-periodic potentials, *Physica A: Statistical Mechanics and its Applications*, **388**, pp. 277-287, 2009.

64. P. R. Kramer, O. Kurbanmuradov, and K. Sabelfeld, Comparative analysis of multiscale Gaussian random field simulation algorithms, *Journal of Computational Physics*, **226**, pp. 897–924, 2007.

65. A.A. Samarskii, *The Theory of Difference Schemes*, Marcel Dekker, New York, 2001.

66. G. W. Griffiths and W. E. Schiesser, *Traveling Wave Analysis of Partial Differential Equations: Numerical and Analytical Methods with Matlab and Maple*, Academic Press, Burlington, USA, 2011.

67. J. Li and Y.T. Chen, *Computational partial differential equations using MATLAB*, CRC Press, USA, 2009.

68. I.K. Shingareva and C. Lizarraga-celaya, *Solving Nonlinear Partial Differential Equations with Maple and Mathematica*, Springer, New York, 2011.

69. G.P. Nikishkov, *Programming Finite Elements in Java*, Springer, London, 2009.

70. H.T. Lau, *A numerical library in Java for scientists and engineers*, Chapman & Hall/CRC, Boca Raton, USA, 2004.

71. R. Mak, *Java number cruncher: the Java programmer's guide to numerical computing*, Prentice Hall PTR, New Jersey, 2003.

72. R. Čiegis, *Diferencialinių lygčių skaitiniai sprendimo metodai*, Technika, Vilnius, 2003.